CHARACTERIZATION OF THE POROSITY AND PORE BEHAVIOR DURING THE SINTERING PROCESS OF 420 STAINLESS STEEL SAMPLES PRODUCED WITH GAS- AND WATER-ATOMIZED POWDER USING POWDER BASED 3-d PRINTING

by

Yu Zhou

B.S, East China University of Science and Technology, 2011

Submitted to the Graduate Faculty of

Swanson School of Engineering in partial fulfillment

of the requirements for the degree of

Master of Science

University of Pittsburgh

2014

UNIVERSITY OF PITTSBURGH

SWANSON SCHOOL OF ENGINEERING

This thesis was presented

by

Yu Zhou

It was defended on

April 2nd, 2014

and approved by

C. Isaac Garcia, PhD, Research Professor

Department of Mechanical Engineering and Materials Science

Qing-Ming Wang, PhD, Professor

Department of Mechanical Engineering and Materials Science

Luis E. Vallejo, PhD, Professor

Department of Civil and Environmental Engineering

Thesis Advisor: C. Isaac Garcia, PhD, Research Professor

CHARACTERIZATION OF THE POROSITY AND PORE BEHAVIOR DURING THE SINTERING PROCESS OF 420 STAINLESS STEEL SAMPLES PRODUCED WITH GAS- AND WATER-ATOMIZED POWDER USING POWDER BASED 3-d PRINTING

Yu Zhou, M.S.

University of Pittsburgh, 2014

A series of 420 stainless steel samples produced using the M-flex system (a powder-based 3D printer) were used to study the systematic evolution of the changes in porosity and pore size behavior after sintering. Powders produced from gas atomization and water atomization have been used to prepare green coupons. The major goals of this work were to; 1) study the optimum sintering processing parameters in terms of temperature and holding time to access the level of densification, 2) develop a better understanding of the relationship between powder characteristics, density, porosity and sintering parameters, 3) investigate the sintering behavior of powders of the same chemical composition but different particle size and distribution.

The microstructural characterization for both gas- and water-atomized powder has been done with the aid of a Scanning Electron Microscope (SEM) and fractal dimension analysis. Different sintering conditions, i.e. temperature and holding time, were examined. The coupon samples were encapsulated in a vacuum quartz tube to avoid oxidation. Shrinkage is measured after sintering, based on which density and porosity are calculated for each sample.

Optical Microscope (OM) has been used to observe the microstructure change in the central part of each sample.

The powder characterization results point out that water atomized powder has a more irregular and complex shape compared to gas atomized powder. Thus it is predicted to have better sintering behavior. The sintering results show that water atomized powder is easier to sinter and can get lower porosity at the same sintering condition compared to the gas atomized powder. However, full densification was not observed under the experimental conditions used in this study. Thus, future studies need to be conducted.

TABLE OF CONTENTS

LIST OF TABLES

LIST OF FIGURES

NOMENCLATURE

D Final particle size of gas atomized powder

D_0 Frequency factor

D_B Fractal dimension

D_{dif} Diffusivity, m^2/s

D_V Volume spherical diameter

G Grain size

$\Delta L/L_0$ Shrinkage percentage

m Mass of a coupon after curing

M_G gas mass

M_M metal mass

$N0$ Total number of atoms

NA Number of active atoms

$N_{B(\varepsilon)}$ Number of boxes with a scale ε

Q Activation energy

Q_B Required energy of breaking the existing bonds

Q_N Required energy to occupy a vacant site

R Gas constant

S Particle surface area

T Absolute temperature

t Time

V Particle volume

V_P Volume occupied by the pores

V_S Volume occupied by stainless steel 420 particles

Greek Symbols

α Other factors coefficient

β Experimental experience coefficient

ε Box size

ρ Density of coupon

ρ_G Green density

ρ_S Sintered density

ρ_s Theoretical density of stainless steel 420

σ_0 Friction stress

σ_Y Yield strength

ψ Sphericity

ACKNOWLEDGEMENT

This research would never be completed without those supports from various kind-hearted people. Here I would like to extend my sincere gratitude to them.

First and foremost, I would like to thank to my advisor, Dr. C. Isaac Garcia, for his great patience and instructive suggestions through my experiments. I would have never accomplished this thesis without his help and guidance.

I would also like to extend my thanks to my committee members: Dr. Qing-Ming Wang and Dr. Luis E. Vallejo, for their time and help to make this thesis better.

Secondly, I would like to thank to my group members, Siw, Sin Chien and Redkin, Konstantin Victorovich, for their useful experience in my research and generous help with my experimental devices.

I would like to thank to Alex Zhang, Yongsen Rong and Patrick Vincent, for their help on experimental works and device maintenance when I was busy with my thesis. And also thanks to all my other friends for their advice and generously standing around me.

I would like to thank to Mr. Schade, Chris in Hoeganaes company to provide the gas- and water-atomized powders, and to the ExOne company, especially to Mr. Orange, Micheal J. for printing lots of samples for the research.

Finally, I would like to thank to my parents for their generous support and encouragements!

Thanks to them all!

1.0 INTRODUCTION

The traditional way to produce engineering materials having complex alloy systems is to melt the homogeneous raw materials mixes into liquid, then cool the liquid metal down until it completely solidifies. After solidification, and depending on the final geometry and required application, the solidified alloyed metal can be subjected to a series of processing treatments, including but not limited to reheating, hot forming, transformation, machining and joining. These series of processing steps are necessary to manufacture engineering components. This has been the traditional way to produce simple and complex metal components used in the industrial world. However, the traditional manufacturing approach to produce engineering components can have high energy cost, long producing period to get final products, and often it is difficult to control the geometry of the parts. Scientists have kept working to find some ways to improve the processing by either reduce the energy consuming and the producing period, or better ways to control complex geometric components.

The recent manufacturing developments on additive manufacturing might provide the opportunity to produce complex engineering components, reduce manufacturing costs and faster delivering time. Additive manufacturing use a Three Dimensional Printing (3D Printing) approach. In 3D printing additive manufacturing, a pre-designed 3D model file is transferred into the additive manufacturing system. The model is then divided into slices in various thicknesses and then it is built layer by layer. Compared to traditional manufacturing, additive manufacturing can produce parts much faster at a lower energy cost, and it can control the

geometry accurately without a die or a mold. However, in accordance to accurate control of complex geometry, the system has high requirements about the powder characterization which leads to a high cost of powder preparation. A huge powder containing and printing system also causes difficulties in replacing powders while other materials need to be printed.

In this thesis, a powder-based 3D printing system called M-flex system has been used to produce the samples. The sintering process of stainless steel 420 printed by this system has been investigated. The relationship between sintering parameters (sintering temperature and holding time) and properties has been studied. The properties of the printing parts are also compared to other stainless steels produced by powder metallurgy.

2.0 LITERATURE REVIEW

2.1 TRADITIONAL MANUFACTURING VS POWDER METALLURGY

2.1.1 Traditional Manufacturing

Traditional manufacturing of steels includes several processes, such as casting, forming, machining and joining.

Casting is a process of pouring liquid steels into a die or a mold with a hollow cavity of certain geometry. The liquid steels will then solidify in the mold and finally form a casting part with a desired shape. Casting is one of the most common processes to produce roughcasts with complex shapes. Compared to the other processes, casting has strong flexibility and adaptability to produce parts of different materials and in different shapes, which makes it good for quantity production in industrial field. However, casting will perform large deviation in size and internal defects, so it is difficult to control the geometry accurately [1].

Forming is a process of producing steel parts by mechanical deformation based on the principle of plastic deformation. There are varies ways of forming process, such as compressive forming (rolling and forging), tensile forming (stretching and expanding), bending and shearing [2]. Forming process requires high loads and stresses, and the shape of

steel parts will be permanently deformed after this process. The mass of a steel part will not change after forming process.

Machining is a process of cutting raw materials into final products with desired shapes, sizes and surface qualities. Unlike forming, machining is a material removal process, so it will always produce some redundant materials which are difficult to reuse. In traditional machining process, certain machine tools such as cutting blades and drilling presses are required to shape the bulk steels. Nowadays advanced technical tools are also added into machining process, such as electrical discharge machining, electrochemical machining and ultrasonic machining. Digital control system can also be applied to machining process to provide more accurate control to the size of steel parts [3]. Machining is an accurate geometry control process and room temperature operation which leads to low energy and time cost. However, there are accuracy limitations in using different tools. What's more, it will always waste certain amounts of materials since machining is a material removal process.

Joining, which refers to welding in most situations, is a process of joining two pieces of parts together, in either the same material or different materials, by melting the contacting point and forming a molten pool where becomes a strong joint after cooling. Various methods can be used to weld materials such as shielded metal arc welding and gas tungsten arc welding, and different energy sources can be used to weld. The welding ability of a material depends on the chemical composition of itself and the welding method, but the chemical composition of the material plays a major role [4]. Take carbon steel as an example. The higher the carbon content, the higher the hardenability which means it is easier to form

martensite leading to hydrogen-induced cold cracking, and therefore the lower the welding ability.

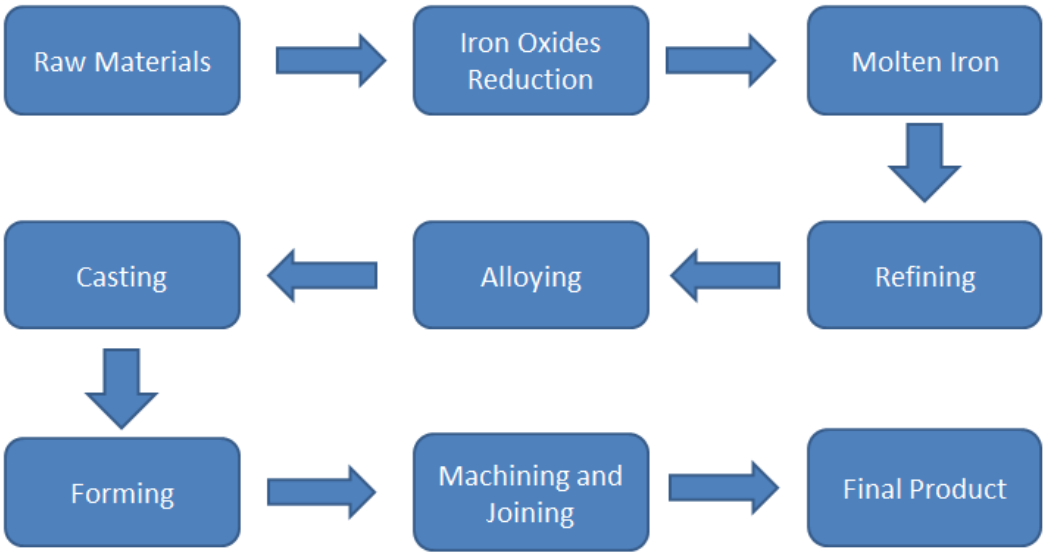

Figure 2.1 Schematic process of traditional steel manufacturing

Figure 2.1 shows a brief route of traditional steel manufacturing process. In general, the traditional way to produce steel parts starts in a blast furnace reducing iron oxides into pig iron which is then molten and reacts with carbon and other additives. The molten steel will solidify through casting process to produce bulk steels, and then follows other manufacturing processes like forming, machining and joining to obtain the final products with certain size and shape. This traditional manufacturing way has several disadvantages. First of all, it consumes huge amount of energy due to several processes that requires high temperature or high pressure. Secondly, it is a long-term producing process from raw materials to final products, which will magnify the first disadvantage of high energy requirement. What's more, certain amount of mass loss exists during this long-term process, especially in machining

process which wastes some materials and induces non-uniform properties. Last but not least, the precision is low in the shape and size control due to the limitation of machining tools.

2.1.2 Powder Metallurgy

Different from traditional steel manufacturing, powder metallurgy (P/M) is a process that converts steel powders into steel products. In this process, steel powders are compacted together in rigid dies at room temperature to produce green parts. Then these green parts are heated following designed heating profiles to form strong bonds between the steel particles, and this process is called sintering. A part produced by P/M process can keep the shape of the die cavity where the powders are compacted, but also improve its strength during sintering.

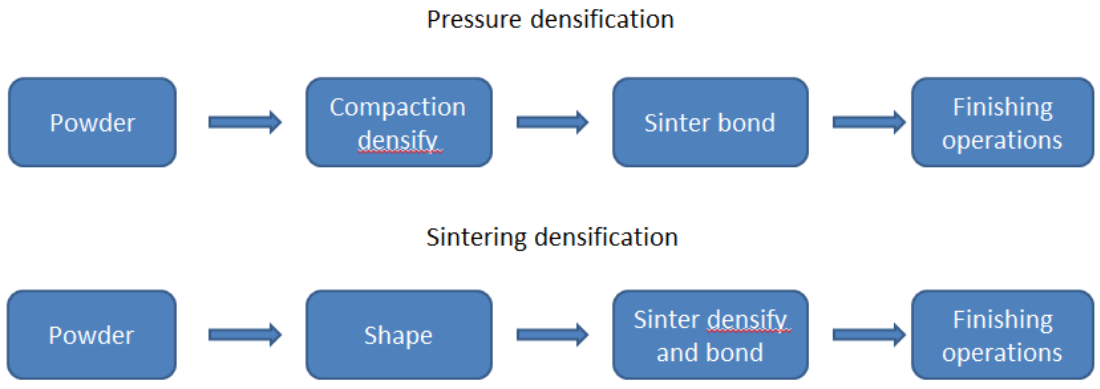

Figure 2.2 Two different concepts of P/M process based on densification occurring step [5]

Generally, the P/M process contains two different concepts according to where the densification occurs. One concept is to compress the steel powders in rigid dies at high pressure to form strong green parts, which is shown as pressure densification in Figure 2.2. In

this case, densification mainly occurs during shaping. The final density increases as the compaction pressure increases, and the dimensions of the final parts are controlled by the rigid dies. The following sintering treatment makes little contribution to densification, but its purpose is to provide a large bonding strength between particles. Therefore, the sintering temperature is low. In the other concept shown as sintering densification in Figure 2.2, external pressure is not applied during powder shaping, which means the powders are looser and the green parts are weaker than the previous case. Unlike the previous one, densification occurs during the following sintering which will result in volume shrinkage. In this case, the sintering temperature is high which leads to pores elimination. These two ends clearly show how compaction pressure and sintering temperature would influence the final products. While determining a profile of P/M process, both pressure and temperature need to be considered in order to get products with good shapes and properties. For example, hot isostatic compaction process applies 200Mpa pressure with a time frame of 1h and a sintering temperature at 800℃ with a time frame of 1h to densify steel powders, while injection molding process applies 14Mpa pressure for 15 seconds and a sintering temperature at 1250℃ for 2h [5].

Compared to the traditional steel manufacturing through the route of casting, forming, machining and joining, P/M process is a more complex process with a higher cost of raw materials and tools, and the remaining pores in the final products will do harm to the properties. However, the advantages of P/M process are also obvious. P/M process consumes lower energy and its production period is shorter. It can achieve better dimensional control in producing more complex shapes with higher precision. The mass loss in the whole process can almost be neglected, which saves more materials. The properties of products by P/M

process are homogeneous and the microstructure is changeable by applying different parameters during compacting and sintering.

P/M process can be divided into three main steps as powder, sintering and finishing [5]. The powder step contains powder production and characterization. The sintering step involves microstructure and property changes, and the selection of parameters and factors such as sintering temperature, holding time and atmospheres. The finishing step is to improve the appearance and properties and it contains various treatments such as surface treatments and heat treatments. Among these steps, sintering is the key step in P/M process, and powder situation has a huge influence to sintering.

2.2 POWDER PRODUCTION AND CHARACTERIZATION

Different processes require steel powders with different sizes and shapes. The purpose of powder production is to produce powders with desired particle size, particle size distribution, and particle shape. There are various techniques to manufacture steel powders, and the atomization technique is one of the most productive and popular route. The basic idea of atomization technique is to deliver energy by a certain fluid to a stream of molten steel, which allows the liquid steel to be separated into droplets and then solidify to form particles. Based on the difference in the fluid selection, the atomization technique can be divided into gas atomization and water atomization, which can fit well in different applications and are always put together for comparison.

2.2.1 Gas atomization

In gas atomization, steels are melted in an induction melter and then pass through a nozzle. High pressure inert gas flowing to the nozzle separates the molten steel into steel droplets which will then solidify while falling into the chamber. In order to prevent the liquid steel from freezing in the nozzle, the required temperature in the melter is much higher than the melting temperature of the steel, which also allows the droplets to form spherical shape before solidification. For steels which are not sensitive to oxidation, melting can take place in the air, otherwise vacuum condition would be required. The inert gas fluid applied in gas atomization is nitrogen or argon in most situations. Figure 2.3 shows a brief schematic process of gas atomization.

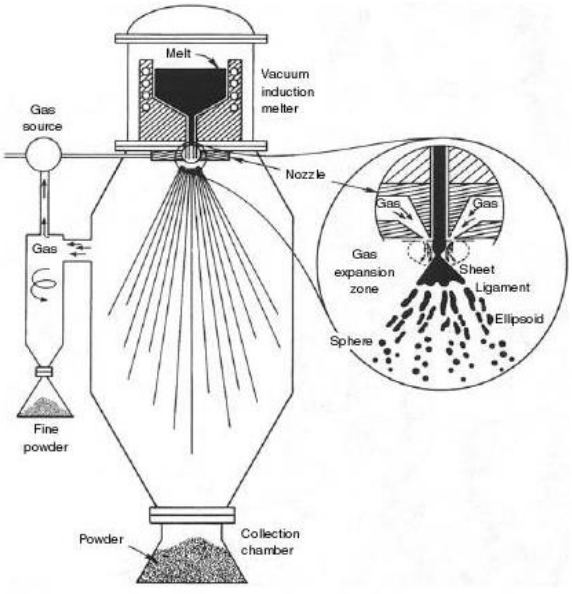

Figure 2.3 Schematic process of gas atomization [6]

In gas atomization, the final particle size depends on different factors, such as metal flow rate, gas energy (which performs as gas pressure and gas flow rate), gas type, nozzle dimensions and liquid metal temperature. Among the above, metal flow rate and gas flow rate play the most important role in determining the particle size. The final particle size D is proportional to the ratio of the metal flow rate to the gas flow rate, and the relationship between them can be approximately expressed in Equation 2.1

$$D = \alpha \frac{dM_M/dt}{dM_G/dt} \qquad 2.1$$

where M_M is the metal mass and dM_M/dt is the metal mass flow rate, and M_G is the gas mass and dM_G/dt is the gas flow rate. The coefficient α in Equation 2.1 represents other factors which will influence the final particle size, including liquid steel temperature, nozzle dimensions, etc. [5]. Therefore, small particle size requires high gas flow rate, which leads to high gas energy and large gas consuming. Gas atomization produces good packing and flowing steel powders in a spherical shape with a size range of 15-300μm. Figure 2.4 shows a scanning electron micrograph of a gas-atomized stainless steel 316L powder.

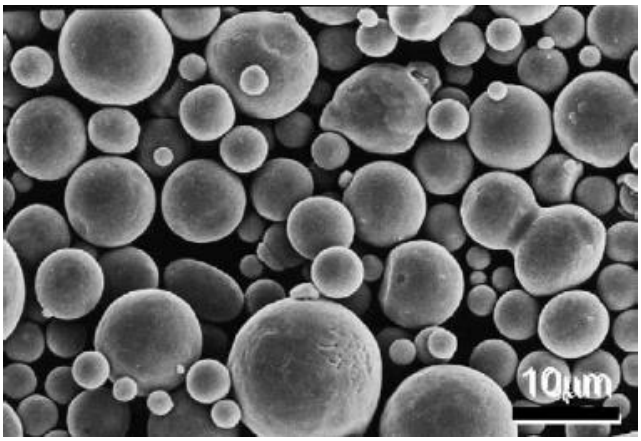

Figure 2.4 SEM picture of stainless steel 316L produced by gas atomization [7]

2.2.2 Water Atomization

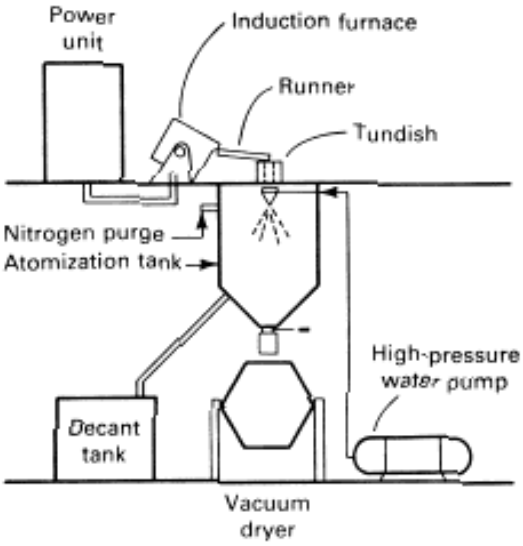

Figure 2.5 Schematic of water atomization [8]

Figure 2.5 is a brief description of water atomization which is similar to gas atomization described in Figure 2.3. In water atomization, high pressure water jets are applied to separate the stream of molten steel into steel droplets while flowing through the nozzle. However, there are two main differences between water atomization and gas atomization.

One difference refers to the particle shape change. Since the thermo-conductivity of water is larger than gas, the heat is extracted faster and the droplets solidify more rapidly in water atomization, resulting in irregular shape and rough surface condition as Figure2.6 shows.

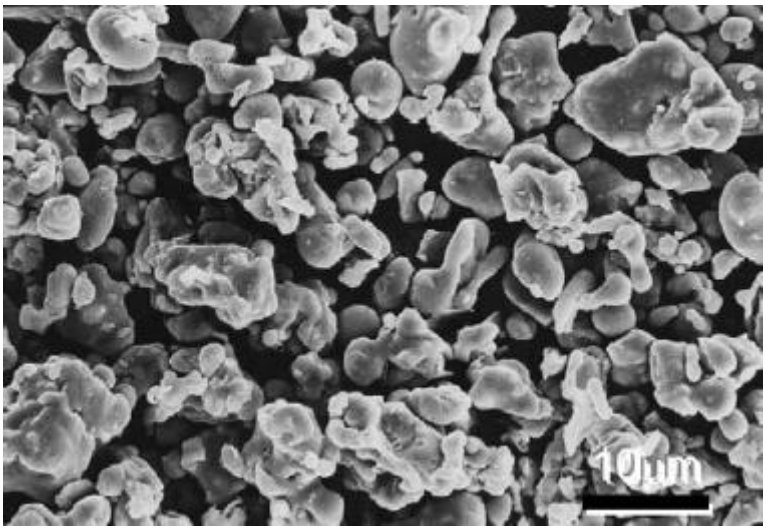

Figure 2.6 SEM picture of stainless steel 316L produced by water atomization [7]

Another difference is oxidation occurring in water atomization. Though the liquid steel after reduction contains low oxygen and the atomization chamber is purged with an inert gas, steel powder will still get partial oxidation due to the reaction between metal and water during solidification as the following chemical reaction describes:

$$xM + yH_2O \rightarrow M_xO_y + yH_2 \qquad 2.2$$

where M refers to a metal element. Therefore, other liquid fluids such as oil have been applied instead of water to reduce the oxidation [9].

Similar as gas atomization, the major factors controlling the final particle shape and size are metal flow rate and water flow rate. Higher water pressure provides higher water flow rate and smaller particle size. There is a typical flow-rate ratio at 5:1 (5 kilograms of water per kilograms of steel powder) in water atomization [5]. Water atomization produces irregular shape powders with a size range of 5-400μm and a lower packing density compared with gas atomization.

2.2.3 Particle Size Characterization

There are various parameters that can measure the particle size, such as maximum and minimum dimension, surface area and mass. Different processes and techniques use different parameters, which is easy to cause misunderstanding. Therefore a standard particle size characterization is necessary to prevent others from being misled. Generally, particle size of a powder is characterized by its mass or its cross-sectional size. A well-known concept to unify the particle size is to transfer the actually measured parameter into an equivalent spherical diameter. For example, if the particle volume V is measured, the corresponding spherical diameter D_V can be determined by the following equation:

$$D_V = (\frac{6V}{\pi})^{1/3} \qquad 2.3\ [5]$$

Sphericity ψ is also widely used to describe the shape of the particles. It is defined as the ratio of the surface area of a sphere with the same volume as the particle to the actual surface area of the particle, as the following equation describes:

$$\psi = \frac{\pi D_V^2}{S} \qquad 2.4$$

where D_V is the equivalent spherical diameter in Equation 2.3 determined by volume measurement, and S refers to the actual particle surface area [5].

Sieve analysis is a simple and widely used way to determine the particle size for larger particles. A sieve contains a mesh with square grids created by equal space wires. The mesh size refers to the number of wires per inch, such as “100 mesh” means 100 wires per inch, which has the same meaning as an opening size of 150μm. Mesh size becomes less accurate while the opening size is going smaller due to the increasing of deviation

compared to the manufacturing tolerances. Therefore sieve analysis is usually applied to determine the particle size larger than 45μm [5]. In sieve analysis, sieves with different opening sizes are piled up one above another, and the opening size decreases from top to bottom. Powders are poured into the sieve on the top and are vibrated for certain time, after which the powders will be separated into different size ranges. For example, the powders with particle sizes larger than 125μm but smaller than 150μm will stay between the 100 mesh sieve and the 120 mesh sieve, while the powders in the size range of 90-106μm will stay between the 140 mesh sieve and 170 mesh sieve. However, this is not very accurate due to different particle shapes. For example, a bar-shape particle with a length of 100μm but a width of 40μm might pass through the sieve with an opening size of 45μm in its length direction. In this case, we can only say that in one direction the particles are below 45μm.

In modern investigation, several advanced technique can also be used to determine particle size with a faster analyzing speed and a more accurate result. Laser light scattering technique is one of them by spreading powders homogeneously in air or water and the light scattering from each particle. The particle size is then determined by measuring the angle and intensity of light scattering [10]. Scanning electron microscope (SEM) can also be used to determine the particle size more intuitively while observing the particle shape and surface appearance. For example, we can tell that the particle size in Figure 2.4 is approximate 5-10μm.

2.2.4 Fractal Dimension

Another way to characterize the particles with complex geometry is using the fractal dimension. The concept fractal was first introduced by B.B. Mandelbrot in 1973 [11] and it is used to investigate the geometry of irregular shapes. In Euclid geometry, people are used to describe the dimensions with an integer, such as a line is in one dimension and a plane is in two dimensions. The difference between traditional geometry and fractal analysis is that fractal analysis does not only use an integer to describe the dimensions. In its point of view, the dimensions should be able to be described in any real number [12]. Take the Von Koch Curve as an example. This curve starts with a straight line. First divide the line into three equal segments. Then draw an equilateral triangle pointing out based on the middle segment, and remove the base segment. Then keep repeating these steps for each segment, a Von Koch Curve will form [13]. This curve will increase one third of its previous length after one process, thus after n times process it is an infinite line since n tens to infinity. If we use a line to measure it, the length would be infinite. If we use a plane to measure it, the value would be zero because a line does not contain a plane. Thus, it has a dimension between 1 and 2.

While using fractal dimension, the fractal dimension D_B of a Von Koch Curve is log4/log3=1.26. Thus, we need to use a tool with a dimension of 1.26 to measure the curve, such as taking a quarter of the whole curve as a ruler with unit length, the length of this curve could be measured as 4. The fractal dimension is a ratio describing how the character of an object will change with the measuring scale changing. It can be used to describe the

complexity of a part, thus it is also a good measurement to describe the irregular particles. A simple way to calculate the fractal dimension is box counting, by using a series of boxes with a size ε to cover the part to be measured, and counting the minimum number of the boxes $N_B(\varepsilon)$ needed to cover it. The fractal dimension D_B can be calculated by the following equation:

$$D_B = \lim_{\varepsilon \to 0} \frac{\log N_B(\varepsilon)}{\log\left(\frac{1}{\varepsilon}\right)} \qquad 2.5[14]$$

2.3 POWDER SHAPING AND COMPACTION

Shaping and compaction are different methods to produce a green part by packing the powders together. As mentioned in Chapter 2.1.2, P/M process can be divided into two different concepts based on densification occurring step. Similarly, shaping is to build up a green part from powders without high external pressure, while compaction means to produce a green part through high pressure in a rigid die.

2.3.1 Shaping

Shaping is an approach to form green parts with complex geometry by adding polymeric binders into steel powders under low pressure. It usually contains four steps: forming a feedstock of powder-binder mixture, shaping the feedstock by certain tools, extracting the binder and sintering densification. Metal powder injection molding (MIM) is a representative example of shaping.

In MIM process, polymeric binder is mixed with steel powders to form a feedstock which is easy to flow into the mold and hold the powder's shape. Since densification relies on sintering step, fine powders smaller than 20μm is preferred in MIM process. Spherical powders provide low viscosity and high packing density, while slightly irregular shape powders provide high compacting strength after debinding [15]. In order to combine the advantages of these two shapes, a nearly spherical shape powder with an aspect ratio of 1:1.2 and a packing density around 60% of theoretical is suggested. A typical composition of 60% powder and 40% binder is applied in powder-binder mixture [6].

The feedstock is then heated above the temperature of the flow temperature of the binder to decrease its viscosity and flows into a mold under a low pressure. After the mold is filled, it is cooled down below the binder's flow temperature so that the binder can hold the powders, which gives the green part certain strength for ejection. After ejection, the binder needs to be removed from the powders by thermal approach in most situations. This can be done by a previous special step for debinding or in the early part of the following sintering step.

MIM process can achieve a 95-98% densification grade [5], or even theoretical density by hot isostatic pressing.

2.3.2 Compaction

Unlike shaping, compaction is a process to shape and densify steel powder. Lubricants are added into steel powder to reduce the friction between external particles and the die wall, which makes the green part easy to eject from the die after compaction. Lubricants will be

burned out during sintering. Compaction will deform the steel particles and cause cold welding at their contacting points which increases the strength of the green part. The density increases as the pressure goes higher, but in actual application tool life need to be considered, which is the limitation of pressure.

There are many approaches in compaction. Uniaxial die compaction is the major approach, but it has limitations to produce green parts with complex shapes. Warm compaction is a good way to improve green part density at lower pressure by heating the steel powder before compaction [16]. Cold isostatic compaction can provide complex shapes by compressing the steel powder in a flexible container which allows pressure to be delivered from all directions.

2.4 SINTERING

Sintering is the most important step in P/M process. It can be defined as a heat treatment that turns the green part into a dense and strong part. During sintering, the particles bonds together which leads to a particle-grain transition, and the grains may increase to a certain size larger than the initial particle size. The steel obtained after sintering shrinks compared to its green state, and always presents a porous structure consisting of grains and pores. The sintering parameters and conditions will directly influence the grain size, the pore size, shape and distribution, and therefore influence the final properties.

2.4.1 Overview

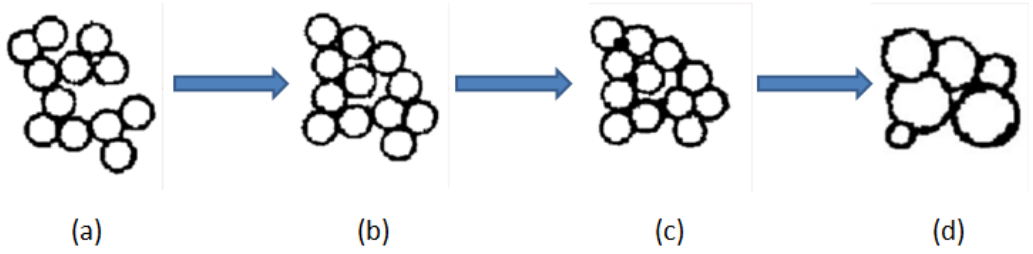

Figure 2.7 A brief description of particle behavior during sintering

Figure 2.7 shows how particles behave during sintering in a brief way. After powder shaping or compaction, the particles touch each other at points and there is some space between particles [17]. In some positions of the green part, the particles may even not touch other particles in every direction and form large vacancies, as shown in Figure 2.7 (a).

In the early period of sintering, the particles are rearranged to eliminate large pores and start bonding together as temperature and time increasing, as shown in Figure 2.7 (b). However, most particles still touch each other at points and the total surface area does not decrease. During this period, binders and lubricants are also removed, which is termed debinding. Most binders and lubricants are polymers with C-C, C-O and C-H bonds with a chemical formula as $C_xH_yO_z$ which will burn out before 650 ℃ and form methane, carbon dioxide, carbon monoxide and water [5]. In order to make sure that the binders and lubricants would be removed totally, the heating rate should be slow during this period.

As the temperature goes on increasing, mass transport stars and the contacting positions between particles grow from points to areas, which means the particles are transferred into grains and the grain boundaries begins forming as Figure 2.7 (c) shows. The total surface area stars decreasing. The pores are still connected with other pores like tunnels in this period.

In the final period of sintering, the grains continuously grow up as the pores shrink and become closed pores. The grain boundaries start moving and most pores on them will eventually disappear at the end of sintering with the highest densification status, as Figure 2.7 (d) shows.

2.4.2 Mechanism

In a green part before sintering, particles are in small size with curved surfaces which are under stress. The total surface area of a green part is large and therefore the surface energy is large, which keeps the green part at a high energy status. During sintering, all curved surfaces will go to flat shape with the least curvature stress, and this is done by atomic motion. Thus, sintering is a spontaneous process because the system always prefers to a lower energy state by decreasing its surface energy to remain stable when particles become easier to move at high temperature. Therefore, the decreasing of surface energy can be regarded as the driving force of sintering, and it is achieved by atomic motion during sintering [18].

Atoms are difficult to move at room temperature for steels, but the mobility of atoms will increase dramatically as temperature goes higher during sintering. The motion

of atoms during sintering needs two conditions. One is that an atom could break the existing bonds with other atoms around it, and another is that a vacant site is available for such atom to occupy. An Arrhenius could be used to describe the relationship between the active atoms N_A and the total number of atoms N_O as follows:

$$N_A = N_O \exp(-\frac{Q_B+Q_N}{RT}) \quad 2.6[5]$$

where Q_B refers to the required energy of breaking the existing bonds, Q_N refers to the required energy to occupy a vacant site, R refers to the gas constant and T refers to the absolute temperature.

Atomic motion during sintering leads to the reduction of surface area and stress by the formation of necks between the contacting particles. Atoms move through different paths which can be divided into surface transport in which the atoms are from pore surfaces, and bulk transport in which the atoms are from the interior of particles. The main difference between these two kinds of transport is that bulk transport results in shrinkage, while surface transport does not cause volume change. Surface transport plays an important role at low temperature by atoms passing along the grain boundaries, which results in strengthening in early period of sintering without densification. In order to densify the green part, the atoms must be transported from the interior of particles to the vacant sites around the contacting points between particles resulting in neck forming. This is mainly controlled by diffusion. The mobility of atoms can be described by the rate of diffusion (termed as diffusivity) using another Arrhenius equation as follows:

$$D_{dif} = D_0 \exp(-\frac{Q}{RT}) \quad 2.7$$

where D_{dif} is the diffusivity measured in m^2/s, D_0 is the frequency factor and Q is the activation energy [19].

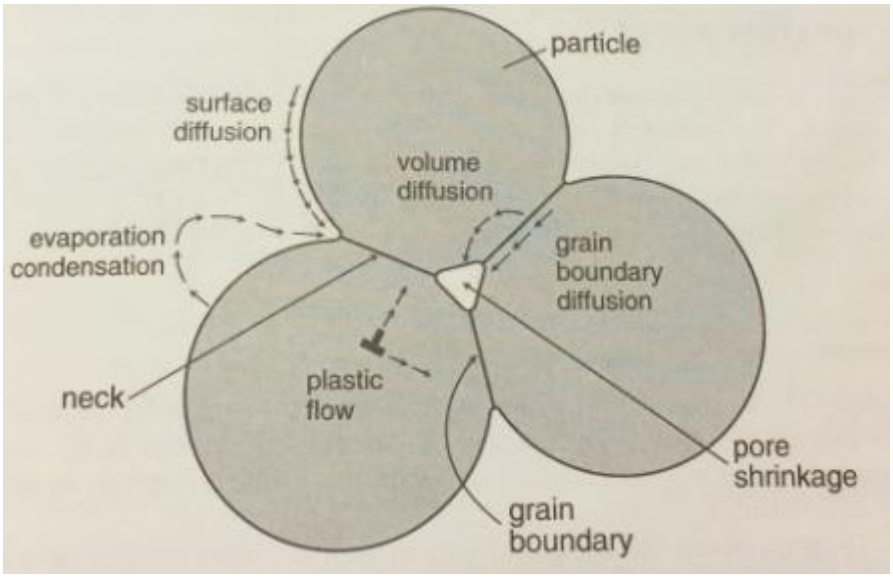

Figure 2.8 Schematic of atomic motion during sintering [5]

Temperature is the major factor influencing the velocity of atomic motion. At high temperature (typically higher than 1120 ℃), atoms can move faster and bulk transport starts to take the major place and makes great contribution to the neck growth by atoms moving through the grain-pore interfaces which makes the pores shrink and results in shrinkage and density increasing. Figure 2.8 shows a schematic of atomic motion during sintering. In this figure, atoms move in various ways of diffusion such as volume diffusion, grain boundary diffusion, and surface diffusion. This figure also shows how grain boundary grows and how pore shrinks during sintering.

However, high temperature and long holding time will not always provide good effects. Though pores would be eliminated during densification, they will also become

smoother and even get larger at high temperature. Eventually the amount of pores decreases but the average size of them increases. The grain size will also increase at high temperature, while the number of grains decreases. The grain size is related to the mechanical properties after sintering, so it needs to be concerned [20].

2.4.3 Microstructure Change

As the previous section has described, the particles combine together to form grains to increase the strength, which is the purpose for sintering and the most important microstructure change in sintering. Besides the change of the bonds between particles, microstructure change during sintering is also represented in the change of pores and grains.

In a green part, binders and lubricants are added to help shaping the powder. When sintering begins, they will be burned out and decompose in early period, and pores are left between the particles. As sintering continues, the pores will eventually be closed without connecting to the outer atmosphere, and the part will not get higher density.

Though the green part would get densification with porosity decreasing during sintering, the pores do not behave simply as shrinking and disappearing. They will change in both shape and size, which is related to the approach applied to make green part, and the sintering parameters [21].

If a green part is made under isostatic conditions, the initial shape of the pores is regular, which results in an isotropic shrinkage during sintering. Sintering shrinkage densify the green part and is related to the density after sintering as Equation 2.8 describes:

$$\rho_S = \frac{\rho_G}{[1-\left(\frac{\Delta L}{L_0}\right)]^3} \qquad 2.8$$

where ρ_S is the sintered density, ρ_G is the green density and $\Delta L/L_0$ is the shrinkage percentage.

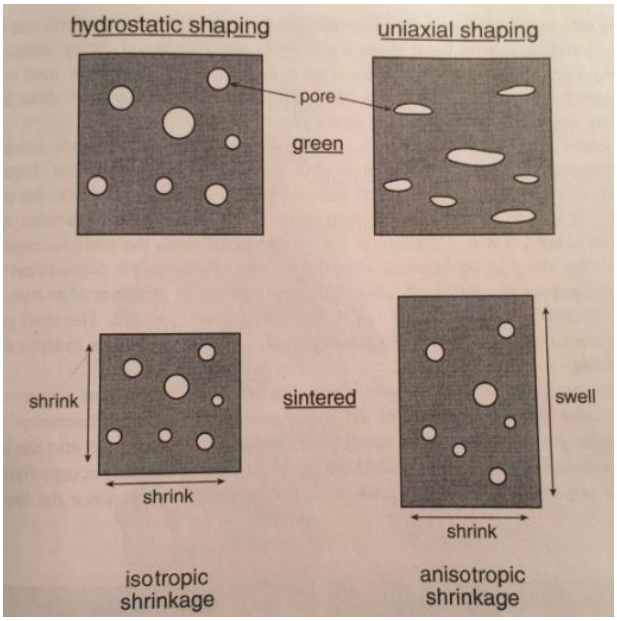

Figure 2.9 Isotropic and anisotropic shrinkage [5]

In contrast, if the green part is compacted under anisostatic conditions such as uniaxial pressing in a rigid die, the particles will be deformed and so as the shape of spaces between particles (pores). In this case, the shape of pores would be like a bar perpendicular to the direction of the pressure. During sintering, these bar-shape pores will change into spherical shape, which means that they will shrink along the length direction but expand in the perpendicular compacting direction. This leads to an anisotropic shrinkage of the part after sintering, which brings difficulty in dimensional control [22]. Figure 2.9 shows the difference between isotropic and anisotropic shrinkage.

Pore coarsening also occurs during sintering. If a green part contains pores with a wide size distribution, the small pores will be eliminated but the large pores will grow in sintering. As sintering goes further, the pore size keeps growing and the number of pores is decreasing, therefore the total porosity of the part is decreasing.

Similar to pore coarsening, the grain size also increases while the number of grains decreases in sintering. Large grain size is not good because it decreases the strength. For example, the relationship between yield strength σ_Y and the grain size G follows the Hall-Petch effect described as the following equation:

$$\sigma_Y = \sigma_0 + \frac{\beta}{\sqrt{G}} \qquad 2.9 \ [23]$$

where σ_0 is the friction stress and β is determined by experimental experience. As Equation 2.7 shows, the larger the grain size, the lower the yield strength. The properties of the sintered steel will increase due to strengthening bonds, but will also decrease due to grain growth. There should be an optimum set of sintering parameters between the two extreme situations.

The rate of grain growth depends on the sintering temperature. If the sintering temperature is too high, grains will grow very fast. The pores will be wrapped into the grains and will not be able to be removed through the grain boundary movement. Therefore, the steel part cannot get higher densification even continuing sintering for longer time.

2.4.4 Sintering Atmosphere

The atmosphere applied during sintering should be able to protect the green part at high temperature by extracting surface oxide and removing burnout binders and lubricants.

In order to protect steel green part, the most concerned points would be the oxidation reduction and carbon content control. At high temperature, iron will react with oxygen as the following chemical reaction:

$$Fe(s) + 1/2O_2(g) \leftrightarrow FeO(s) \qquad 2.10[5]$$

where s and g stand for solid state and gas state. This reaction can go both ways, showing that a low partial pressure of oxygen leads to iron oxide reduction (pushing the reaction to the right side). Iron oxide also reacts with hydrogen and carbon monoxide as follows:

$$FeO(s) + H_2(g) \leftrightarrow Fe(s) + H_2O(g) \qquad 2.11[5]$$

$$FeO(s) + CO(g) \leftrightarrow Fe(s) + CO_2(g) \qquad 2.12[5]$$

These two chemical reactions state that a high partial pressure of hydrogen or carbon monoxide leads to iron oxide reduction, while a high partial pressure of water vapor and carbon dioxide leads to iron oxidation. Therefore, the purity of atmosphere is very important.

Similar principles can be applied to control the carbon content during sintering through atmosphere selection. The general reactions between iron and iron carbide during sintering are described as following:

$$3Fe(s) + 2CO(g) \leftrightarrow Fe_3C(s) + CO_2(g) \qquad 2.13[5]$$

$$3Fe(s) + CH_4(g) \leftrightarrow Fe_3C(s) + 2H_2(g) \qquad 2.14[5]$$

$$Fe_3C(s) + H_2O(g) \leftrightarrow 3Fe(s) + CO(g) + H_2(g) \qquad 2.15[5]$$

By controlling the partial pressure of carbon monoxide, carbon dioxide, methane, hydrogen and water vapor, the carbon content could be graded.

There are several choices for P/M sintering atmosphere, such as pure hydrogen, nitrogen-hydrogen gas mixture, dissociated ammonia, endothermic gas and vacuum [9].

Pure hydrogen has a good thermal conductivity and it can react with oxygen to form water, which do great contribution to sintering by reducing the metal oxides. Take stainless steel as an example. In stainless steel, chromium protects it from being corroded by forming a coat of chromium oxide. However, the temperature required for sintering this oxide is higher than the melting temperature of stainless steel. In this case, pure hydrogen can be used to reduce chromium oxide and make stainless steel much easier for sintering. Pure hydrogen is flammable and explosive, so safety should be the first concern while using this atmosphere.

Nitrogen is a neutral atmosphere and it can do benefits to many steels by residual in the steel to increase strength. It is usually applied in sintering with other gas additions due to its low cost, such as nitrogen-hydrogen gas mixture. This mixture is not flammable with the content of hydrogen below 5%, which is safer than pure hydrogen. However, if the steel being sintered contains titanium, aluminum, chromium and tantalum, nitrides will form and decrease the properties after sintering.

Dissociated ammonia is a mixture with a 3:1 ratio of hydrogen to nitrogen formed by decomposition of NH_3 as follows:

$$2NH_3(g) \rightarrow 3H_2(g) + N_2(g) \qquad 2.16$$

Since this decomposition reaction takes place at high temperature near 1000 ℃, it will provide a purer atmosphere of hydrogen and nitrogen as a reduction gas mixture.

Endothermic atmosphere is produced by catalytic reaction of 93%methane and air which forms nitrogen and hydrogen mixture with water, carbon monoxide and carbon dioxide.

Vacuum condition creates a non-reactive environment for sintering due to continuously pumping to extract all the forming gas out of the furnace chamber. Under this condition, heat is transferred to the green part only through radiation. Vacuum condition can be applied to sinter most of the steels, but it may not be the best choice to achieve the optimum final properties.

2.4.5 Sintering profile examples and related researches

Sintering profiles are various for different steels due to their different compositions, characteristics and special requirements for properties.

Stainless steels can be sintered at 1250-1365℃ with a heating rate at 5-10℃/min under pure hydrogen atmosphere or vacuum condition. C. C. Degnan, P. Jackson, D. P. Weston and J. V. Wood have done research on stainless steel 316L sintering process. They compact the stainless steel powders by uniaxial pressing with a rigid die, and then they use reactothermitic sintering (RTS) to sinter the green part. This method can achieve full density after sintering [24]. O. Ertugrul, H. S. Park, K. Onel and M. Willert-Porada have investigated the effect of particle size and heating rate for sintering stainless steel 316L in microwave under an atmosphere of 90%Ar + 10%H_2, stating that a particle size of -45μm and a heating rate at 15K/min will be the optimum in microwave sintering of stainless steel 316L [25]. Effects of sintering temperature [26] and atmosphere [27] on the structure and

properties have also been studied. The densification increases with temperature, and argon atmosphere provides better densification than nitrogen. The effect of additions such as YAG has also been studied [28].

Iron-carbon steels can be sintered at 1100℃ for 30min under high nitrogen atmosphere due to their high diffusion rates. Reactive sintering for Nickel monoaluminide coating on ultralow carbon steel has been studied [29]. Laser sintering of high carbon steel related to the carbon content has also been investigated [30]. Research has also been done on liquid phase sintering of high carbon steel [31,32].

Alloy steels with high green density can be sintered at 1120-1150℃ for 20-30min under reducing atmosphere, while low green density steels being sintered at 1250℃. High temperature wetting and infiltration for low alloy steel liquid sintering has been studied [33]. Effect of Nickel nanoparticles to low alloy steel sintering has been investigated [34].

Tool steels can be sintered near 1250℃ under vacuum condition. Sintering route for cold work tool steels has been optimized [35]. A spark plasma sintering to produce a hybrid tool steel has also been developed [36].

2.5 ADDITIVE MANUFACTURING

Additive manufacturing (AM) is a process with a brand new concept to produce a three dimensional part from a digital model designed through computer software without any process planning. In AM process, a digital model of the desired part designed by a three-dimensional (3D) computer-aided design (CAD) software is converted into a surface

tessellation (STL) file. The STL file is then transferred into an AM system for analysis and set-up. AM system divides the model into slices as a series of cross-sections, and then build the part up layer by layer. There are several examples of AM process.

Photopolymerization process is one of the AM processes applied to produce photopolymer parts. Photopolymer will react and solidify by irradiation in the ultraviolet range of wavelengths. Thus, AM process can be achieved by controlling the radiation [37]. Figure 2.10 shows three different approaches of photopolymerization process, involving vector scan (approaches of commercial stereolithography machines), mask projection (solidify the entire layers at one time) and two-photon with high resolution.

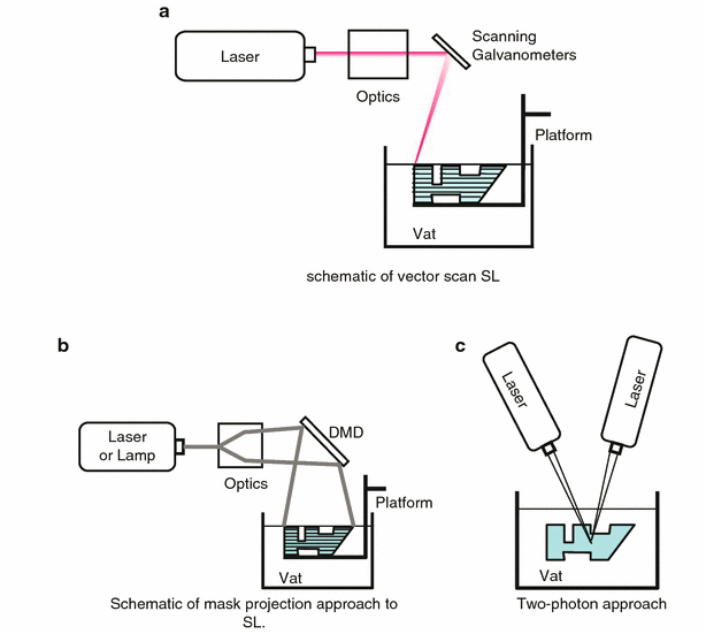

Figure 2.10 Three approaches of photopolymerization process [38]

Another process called selective laser sintering (SLS) process is based on the concept of powder bed fusion (PBF) [38]. A thin layer of powder is spread into the

working area in a chamber filled with nitrogen gas and a roller is applied to flatten the powder layer. The powder layer is heated to a certain temperature below its melting point after which a carbon dioxide laser beam will be focused on the powder layer to sinter the first slice cross-section. After the first layer is done, the working platform will go down for a layer thickness and the second layer is spread by the roller, following the previous steps as cycles for the remaining layers. Figure 2.11 shows the schematic of SLS process.

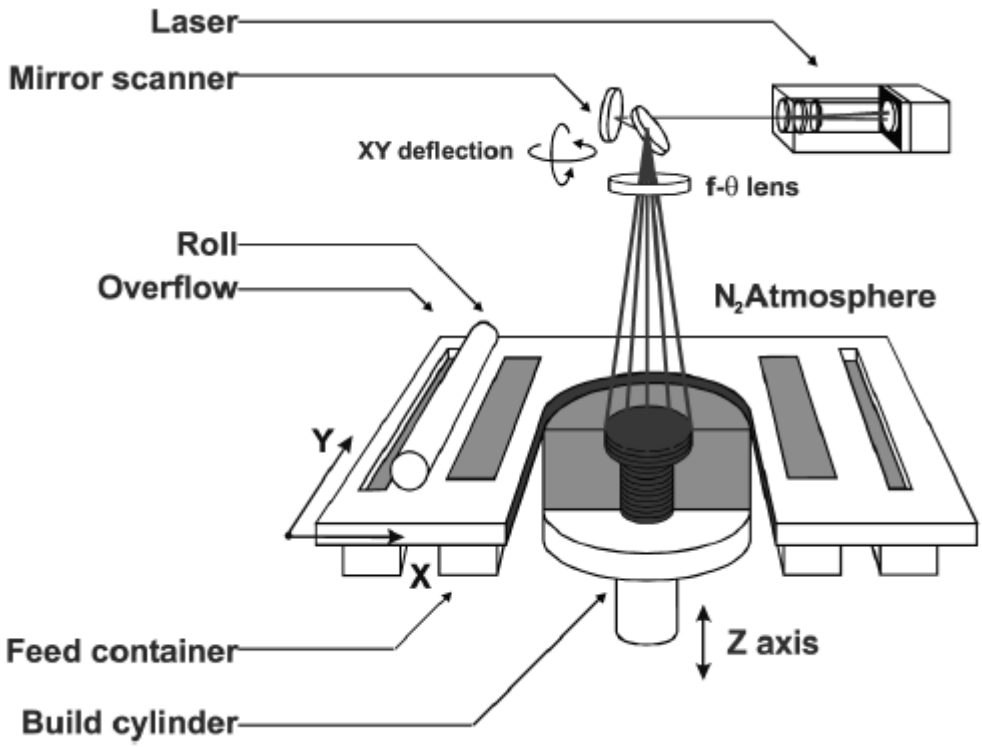

Figure 2.11 Schematic of SLS process [39]

Other processes such as 3D printing process, sheet lamination process and beam deposition process are also included in AM process.

AM process contains several advantages compared to traditional manufacturing processes. First of all, it has a freedom of choosing materials and designing models on

demand without tools limitations. Secondly, the manufacturing speed is very fast compared to the long-term processing in traditional way, and the cost is lower than the traditional manufacturing, either in economical concern or energy concern. What's more, it has a good control of size and shape with complex geometry. These advantages make it convenient for everyone to schedule his or her own manufacturing in a factory, or in a store, or even at home.

Research has been done to investigate the probability to control the porosity of materials by AM process. A 3D Printer is used to prepare the sample and titanium has been selected to print as a dental implant. The result of this research states that the shrinkage increases as the temperature goes higher, and the porosity has a great difference between the surface and the internal [40].

3.0 RESEARCH OBJECTIVES

Additive manufacturing process provides an accurate control of the size and geometry of a part. Thus, AM process can be introduced into P/M process for better dimensional control. In this thesis, a powder-based 3D printer was applied to produce a set of stainless steel 420 green coupons using two different powders of the same chemical composition. One set of powders was prepared by gas atomization techniques, while the second type was prepared by water atomization techniques for comparison purposes. This thesis focuses on the sintering behavior of the 3D printed stainless steel coupons.

According to the sintering mechanism, sintering is a process for green parts made of powders to get densification and high strength. Therefore, the primary goal of this thesis is to determine an optimum sintering process to obtain low porosity for both types of powders. In addition, a second goal of this thesis is to examine the difference of sintering behavior between gas atomized powder and water atomized powder. During sintering, the shape and size of pores are changing which will also influence the sintering process, thus the microstructure change during sintering is also observed and analyzed.

In general, the objectives of this thesis can be summarized as:

1. To determine the optimum sintering profiles for both gas and water atomized powder.

2. To describe the difference between the sintering behaviors of gas atomized powder and water atomized powder.

3. To describe the microstructure change during sintering process.

4.0 EXPERIMENTAL PROCEDURE

4.1 GREEN PARTS PREPARATION

4.1.1 Powder Characterization

Stainless steel 420 powders made by gas atomization and water atomization with an average size about 30μm are used to prepare the green parts, respectively. Scanning electron microscope (SEM) images have been taken to observe the powders appearances in a micro-scale. This is done by dispersing small amount of powder in one droplet of ethanol on a piece of conducting resin pasted on a 1 inch diameter copper cylinder as a plate for observing and then drying the ethanol, An image-analysis software called Image J has been applied to analyze the graphs and a plugin of this software called FracLac has been used to determine the fractal dimension of each kind of powder.

SEM is an electron microscope that can provide good resolution at high magnification. It consists of vacuum system, electron beam system and image formation system. The sample in SEM is scanned by a focused electron beam which interacts with atoms and produces detectable signals such as secondary emitted electrons and backscattered electrons carrying various information of the sample, such as surface appearance and chemical composition. Thus, detections of different signals can show different properties of the sample.

Image J is an image processing and analysis software developed by Rasband, W.S. in 1997 [41]. It is written in Java and can be run on various systems. It can provide different treatments to the images, such as enhancement, geometric operations, particle analysis and color processing. Various plugins can be loaded into this software for further analysis and specific applications.

FracLac is a plugin for Image J for digital image analysis of morphological features developed by Karperien, A. in 1999 at Charles Sturt University. It is often used for fractal and lacunarity analysis [42].

4.1.2 Shaping by 3D Printer

A powder-based 3D printing system called the M-Flex 3D Printer shown in Figure 4.1 is introduced to shape the green samples of the two stainless steel 420 powders. This is an AM system producing parts with complex geometry directly from a .stl file, and various materials can be printed by this system, such as glass, ceramics and metals. It has a 400mm x 250mm x 250mm building space inside a job box and can achieve a building speed of 30 seconds per layer. The reason why this system is called a powder-based system is that, the part after printing is still a powder piling up part which needs following heat treatments.

Figure 4.1 M-Flex 3D Printer

The M-Flex 3D Printer can be divided into four parts, the job box, the powder spreading part, the binder jetting part and the controlling software. The job box is a container with a mobile plate inside called printbed which can be moved up and down. It is set in the working zone where powders will be sprayed. The powder spreading part contains a hopper where powders are dumped in, a recoater with heating elements which gets the powders from the hopper and spreads thin layer powders on the printbed, and a sensor detecting the amount of powders in the recoater, as shown in Figure 4.2(a). The binder jetting part connected to the binder and cleaner consists of a printhead which sprays binder into the powder layer while passing over the working area, and a swipe for cleaning and maintenance of the printhead, as shown in Figure 4.2(b). The controlling software is linked to the previous two parts to control the whole process of printing.

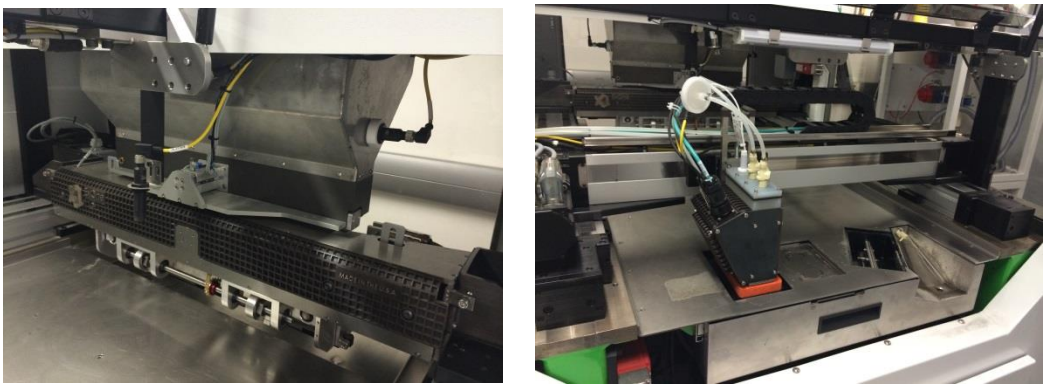

(a) (b)

Figure 4.2 The hopper, recoater and printhead of 3D Printer: (a) hopper and recoater, (b) printhead

Before printing, some preparations have to take place. The job box needs to be engaged in the system and the printbed should be lifted to the top. Several foundation layers are spread and pre-heated as foundation layers for building up the parts. The printhead goes through the prime, wipe and jet process and prints test patterns to ensure that it is good enough to work. Stl digital 3D models for printing are transferred into the software and are loaded in the working area in the printing setup window as a preview. In this section, the parts can be moved and rotated to arrange them in any position of the working area, and can be shrunk or expanded to the original size in all dimensions by imputing three scale factors in each of the x, ,y and z direction respectively. The printing parts are analyzed and cut into certain amount of slices for the following layer-by-layer building according to their thickness. After all these preparations finish, the printing is ready to go. First, the recoater goes through the whole printbed heating it to a temperature around 60℃ and spreads the first layer of powder on its way back. Then the printhead travels through certain working area depending on the printing slice and sprays binder in a pattern same as the cross-section of this slice to bind selected areas of powders after which the first layer is done. The recoater then goes

through the printbed again, drying the sprayed binder and spreading the second layer of powder on its way back. These steps will run as a cycle to build up the parts layer by layer until the job finishes. During printing, the binder saturation was set to 55%, which means the binder would occupy 55% volume of the space between particles.

After the printing finishes, the printbed will be moved to the botoom of the job box. The job box is then transported into an oven for curing at 195℃ (383℉) to evaporate the solvent in the binder and obtain the primary strength for picking up. During curing, the other powders stay in the job box as a support to the green parts. After curing, the green parts are ready for sintering process.

In this thesis, 12.7mm x 12.7mm x 5mm coupons are printed for the ease to observe the shrinkage in different directions. After printed, they are cured at 195℃ for 8 hours.

4.2 SINTERING

4.2.1 Sintering Conditions

After curing, the coupons are encapsulated in quartz tubes under vacuum condition separately. Since the binder has been burn out during curing, quartz tube encapsulation would be an easy way to achieve vacuum condition for small parts sintering in this case.

A programmable tube furnace with a maximum working temperature at 1600℃ and a maximum temperature ramping rate at 10℃ /min is used for sintering. A computer is

connected to the temperature controller of the furnace to program and monitor the heating curve. Up to 30 segments can be input for each program.

4.2.2 Sintering Temperatures and Holding times

As explained in the previous chapter, the sintering temperature and holding time will be different based on various shaping and compaction approaches. If the green part is formed through high pressure compaction, the sintering temperature is not high (in a range of 1120-1150℃) and the holding time is short (i.e. 60min) [5, 9]. If the green part is formed through low pressure shaping such as MIM process, the sintering temperature is higher than the previous case (in a range of 1200-1360℃) [5, 7, 9] and the holding time may also be longer (i.e. 90-180min). In our case, the green part is prepared by a powder-based 3D printer. From the introduction in section 4.1.2, the green part is only bonded together with the help of binder and no external pressure is applied, so high sintering temperature and long holding time are needed. Since the quartz tube cannot suffer above 1300℃, the two sintering temperatures are determined at 1250℃ and 1300℃ and the starting holding time is determined at 540 ℃min. Usually the heating rate should not exceed 5℃/min in order to burn the binder out completely, so the heating rate is determined at 5℃/min.

In this thesis, five sets of sintering parameters were examined. The first sintering process is described as follows:

1. Raise the temperature from room temperature (25℃) to 420℃ at a heating rate of 5℃/min.
2. Hold the temperature at 420℃ for 30min.

3. Raise the temperature from 420 ℃ to 630 ℃ at a heating rate of 5 ℃/min.

4. Hold the temperature at 630 ℃ for 60min.

5. Raise the temperature from 630 ℃ to 1250 ℃ at a heating rate of 5 ℃/min.

6. Hold the temperature at 1250 ℃ for 540min.

7. Cool down to room temperature at a cooling rate of 5 ℃/min.

This sintering profile is also plotted in Figure 4.3.

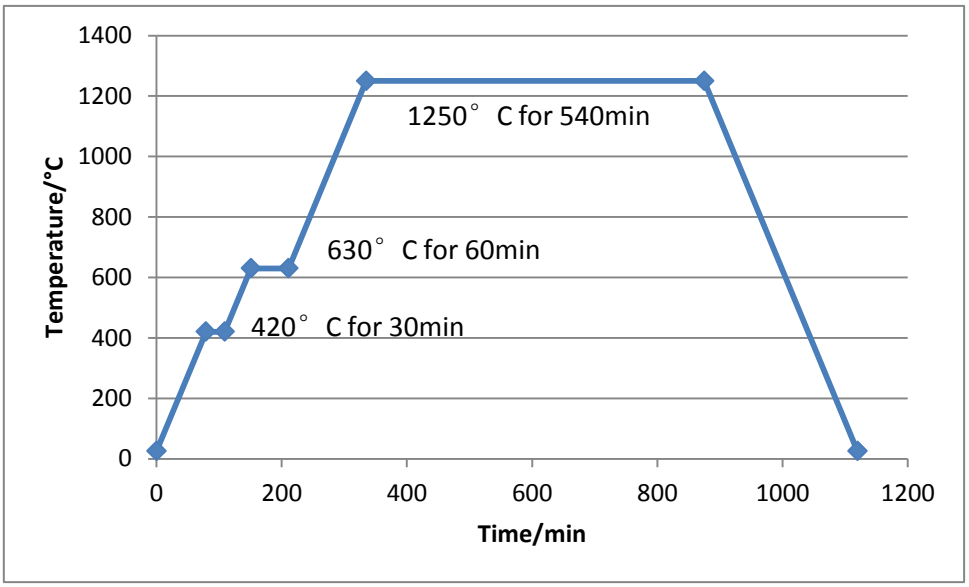

Figure 4.3 Sintering profile at 1250 ℃ for 540min

The following two sintering are processed in the same way as the first sintering, except for increasing the holding time in step 6 to 1000min and 1200min. Holding times for 540min and 1200min are also processed at 1300 ℃ for comparison. Every sintering process is applied to the coupons made of both gas atomized powder and water atomized powder.

4.3 MICROSTRUCTURE ANALYSIS

4.3.1 Optical Microscopy

After sintering, the coupons are cut along the layers building up direction by a diamond blade cutter, and the cross-sections are observed by Optical Microscope (OM). The OM we used in our research is a digital optical microscope (Keyence, VHX-600) which can provide a bright background by setting white balance and a strong color contrast by setting image enhancement. For each coupon, OM pictures have been taken at different magnifications.

4.3.2 Image Software Analysis

The OM pictures are analyzed by Image J to measure the porosity and determine the pore size and distribution.

5.0 RESULTS AND DISCUSSIONS

5.1 POWDER CHARACTERIZATION

5.1.1 Gas atomized powder

The microstructural descriptions of the particles prepared using gas atomization are shown in Figure 5.1. These pictures show the shape of the 420 stainless steel particles prepared using gas atomization procedures at different magnifications.

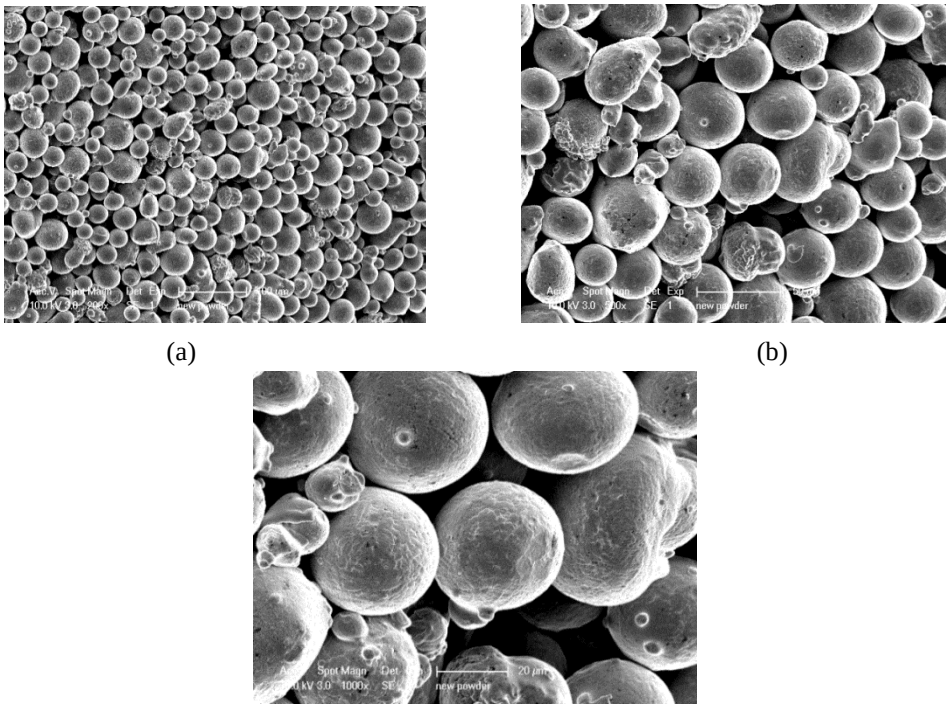

(a) (b)

(c)

Figure 5.1 SEM images for gas atomized stainless steel 420 powder at different magnifications: (a) 200x magnification, (b) 500x magnification, (c) 1000x magnification

Figure 5.1 (a-c) show the SEM images of gas atomized powder under 200, 500 and 1000x magnification, respectively. From these images, it can be observed that most of the particles in this gas atomized powder are nearly spherical in shape with an average size around 30μm. The gas atomized powder has a good packing ability and the spaces between particles are very small compared to the particle size, as shown in Figure 5.1(a). This homogeneous compact packing will lead to isotropic shrinkage. Few particles with non-spherical shape can be observed in Figure 5.1(b). Small number of particles approximate to or smaller than 10μm can be observed in Figure 5.1(c).

Fractal analysis for gas atomized powders has also been done by FracLac. Since this analysis requires a binary color system between the analyzing target and the background, particles in Figure 5.1(c) at 1000 magnification has been picked up and threshold color has been adjusted to clearly show the difference between particles and background before analysis scanning. This scanning is based on standard box counting method in fractal dimension calculation as mentioned before. The fractal dimension of this gas atomized powder is measured as 1.03, stating that the shape is almost spherical because the fractal dimension of a sphere is considered as 1.

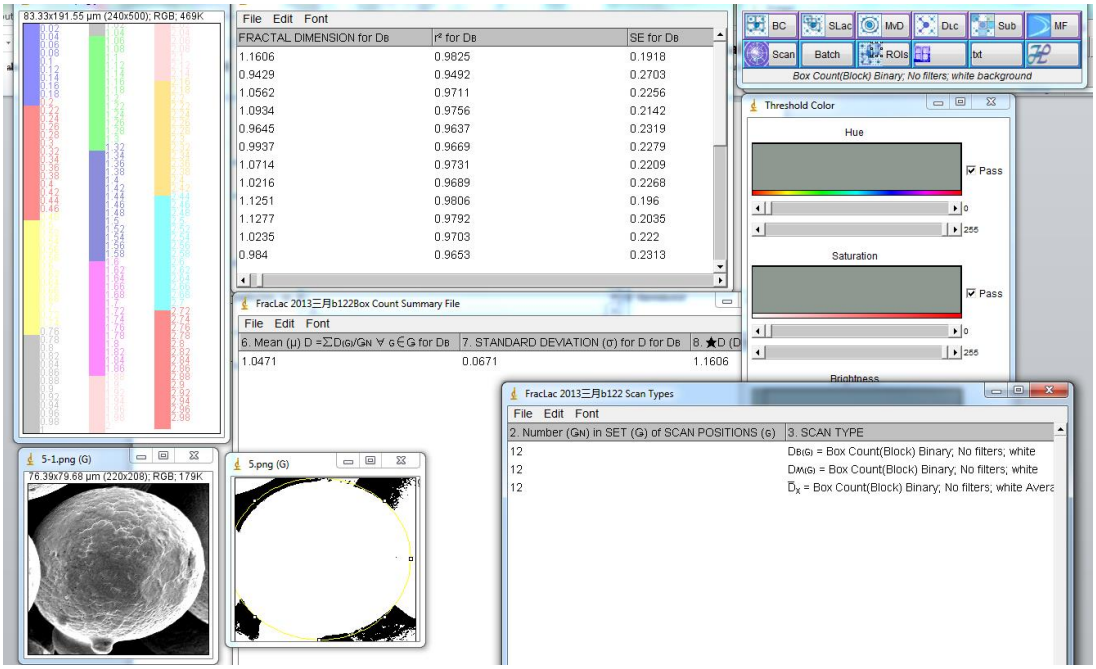

Figure 5.2 Example of fractal analysis using FracLac

Figure 5.2 shows an example of how fractal is analyzed. The method involves the selection of a good particle. Then adjust the threshold to increase the contrast and make the image binary. Then select the particle and do the box count scanning. The results will be presented in several tables including the fractal dimension D_B, standard deviation σ, etc.

5.1.2 Water Atomized Powder

The SEM characteristics of the stainless steel 420 powder prepared using water atomized process are presented in Figure 5.3. The SEM micrographs of the water atomized powder clearly show the irregular shape of these particles compared to the regular (spherical) shape of the particles produced by gas atomization.

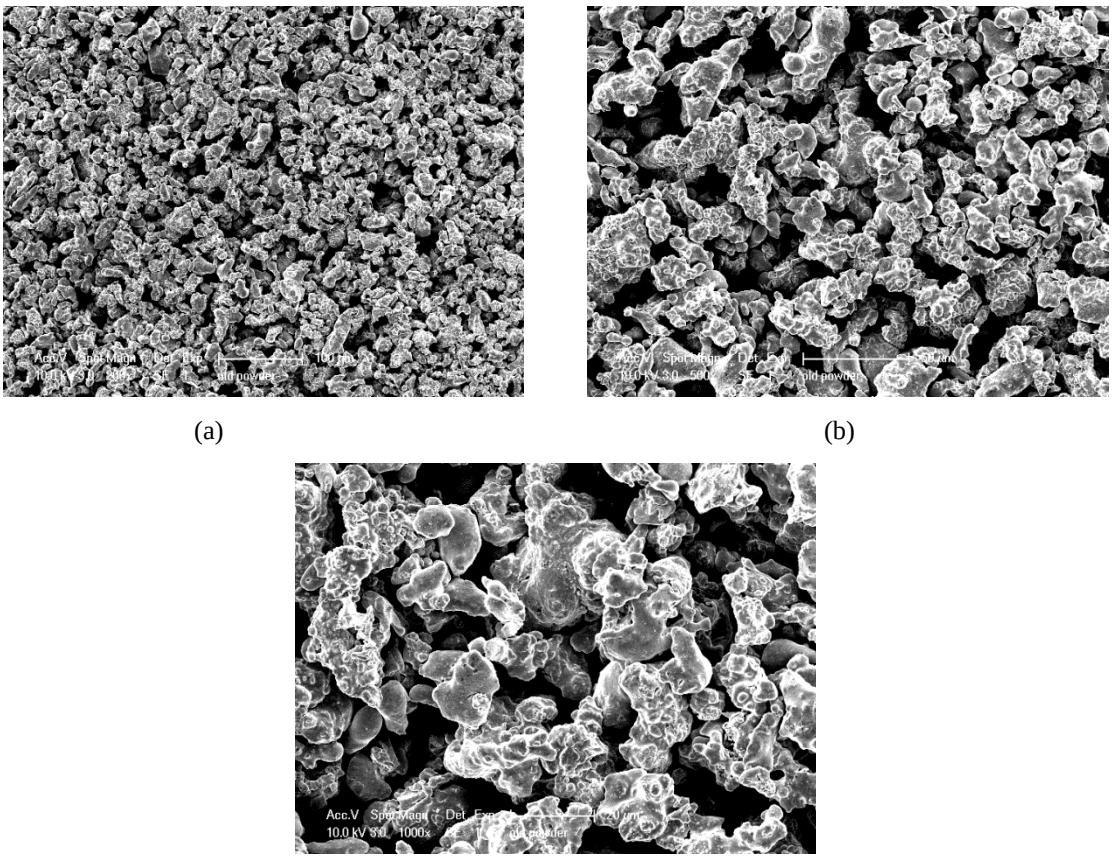

(a) (b)

(c)

Figure 5.3 SEM images of water atomized stainless steel 420 powder at different magnifications: (a) 200x magnification, (b) 500x magnification, (c) 1000x magnification

The SEM analysis and fractal analysis have been done for water atomized powder. Figure 5.3 (a-c) shows the SEM images of water atomized powder at different magnifications. This group of images shows that the particles in water atomized powder have irregular shapes. They may be long in one direction but short in another. It can also be observed that they do not have good packing ability because the spaces between particles are large compared to the particle size. In other words, they pack together in a loose way. The particles do not pack together homogeneously due to their irregular shape, which will lead to anisotropic shrinkage.

Fractal analysis result states that the fractal dimension of water atomized powder is 1.70, representing that the shape of the particles is irregular and complex. However, due to

the irregular and complex shape, the surface area of water atomized powder is larger than the gas atomized powder, and therefore water atomized powder has a higher surface energy than gas atomized powder. However the difference in packing and shape of the particles might provide a higher driving force for sintering. For example, the decreasing of the total surface energy of the system can be regarded as the driving force of sintering process, the coupons made of water atomized powder should exhibit faster kinetics of sintering than the coupons made of gas atomized powder.

5.2 POROSITY

In this section, the shrinkage and porosity for each sample is calculated, and the OM pictures are taken to see the internal microstructure change. Area porosity obtained through the OM images are compared to the body porosity to show the mechanisms of pore movement during sintering.

5.2.1 Porosity before sintering

After sintering, the coupons have a light gray color which means that oxidation is avoided during sintering. The coupons after sintering are shown in Figure 5.4. From this figure it can be observed that the water atomized coupon (right) has a large shrinkage than the gas atomized coupon (left), but both of them keep their shape.

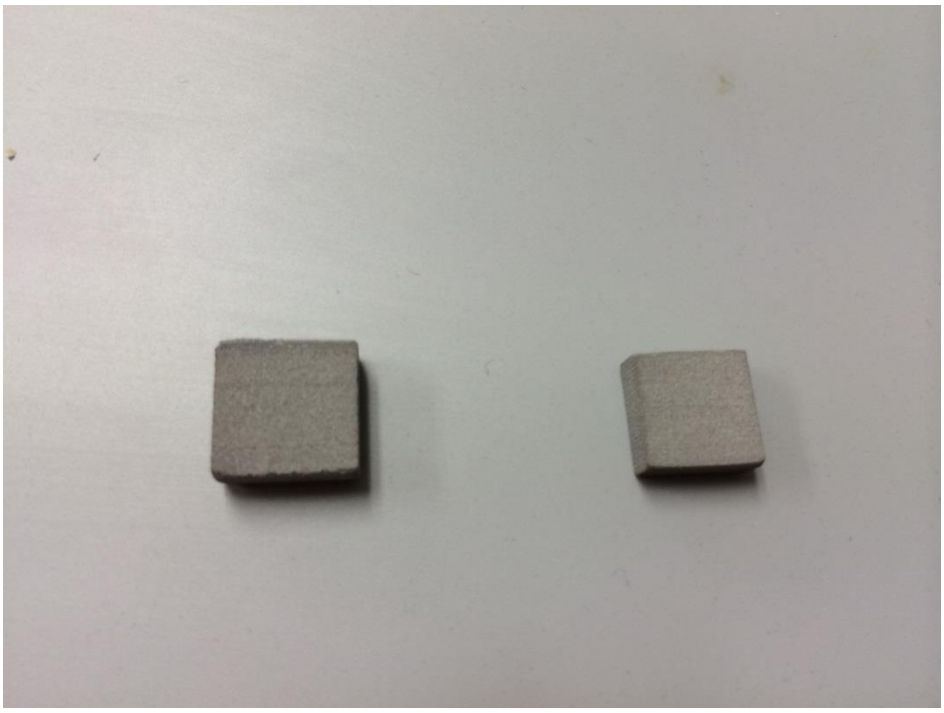

Figure 5.4 Gas atomized coupon and water atomized coupon after sintering

The mass and dimensions of each coupon after curing is measured and average data have been calculate to characterize the porosity of each powder before sintering. The relationships between the mass of a coupon after curing, m, the volume occupied by stainless steel 420 particles in the coupon, V_s, the volume occupied by the pores, V_p, the theoretical density of stainless steel 420, ρ_s, and the density of the coupon, ρ, can be represented as following relations:

$$\rho = \frac{m}{V_s+V_p} \quad 5.1$$

$$\rho_s = \frac{m}{V_s} \quad 5.2$$

Divide Equation 5.1 by 5.2 and then subtracted by 1, the porosity of the green part can be calculated as:

$$1 - \frac{\rho}{\rho_s} = \frac{V_p}{V_s+V_p} = Porosity \quad 5.3$$

The density of each coupon is easy to calculate by measuring the mass and dimensions due to its simple shape. Since the theoretical density of stainless steel 420 is

known as 7.75g/cm^3, the porosity can be calculated. The average density and porosity of coupons before sintering are shown in Table 5.1.

Table 5.1 Porosity before sintering

	Gas atomized coupon	Water atomized coupon
Density (g/cm^3)	3.96	3.62
Porosity (%)	48.91	53.30

The data in Table 5.1 show that gas atomized powder have better packing ability than the water atomized powder.

5.2.2 Porosity at 1250 ℃

The mass and dimensions of each coupon sintered at 1250 ℃ are measured. The shrinkage percentage, density and porosity are calculated and listed in Table 5.2 and Table 5.3. The porosity vs holding time plot is shown in Figure 5.5

.**Table 5.2** Shrinkage percentage, density and porosity of gas atomized coupons after sintering at 1250 ℃

Time/min / Properties	540	1000	1200
Shrinkage(%)	9.99	18.83	19.41
Density(g/cm^3)	4.27	4.73	4.76
Porosity(%)	44.91	38.97	38.59

Table 5.3 Shrinkage percentage, density and porosity of water atomized coupons after sintering at 1250 ℃

Time/min / Properties	540	1000	1200
Shrinkage(%)	38.43	44.91	45.86
Density(g/cm^3)	5.70	6.37	6.49
Porosity(%)	26.46	17.81	16.26

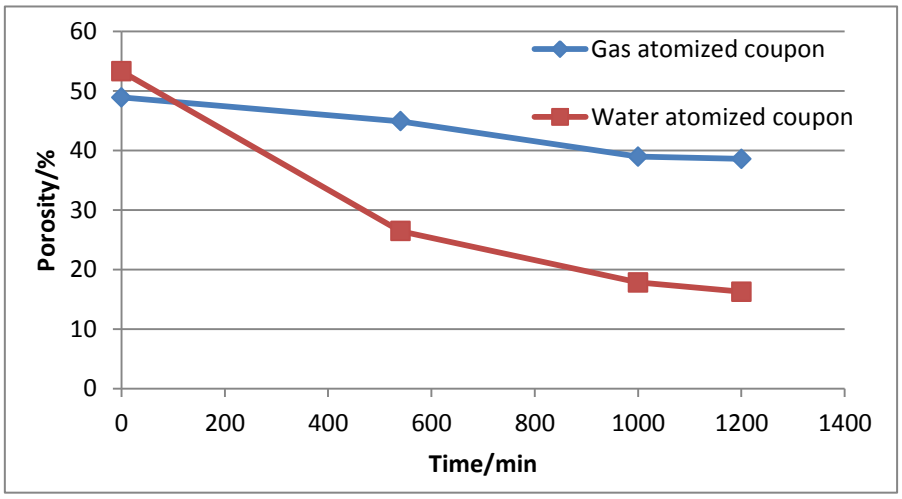

Figure 5.5 Porosity change with holding time for gas- and water-atomized powder

In Figure 5.5, the porosity of both gas- and water-atomized powder decreases as the holding time increases before 1000min, stating that certain holding time is necessary for high densification. What's more, both curves drop quickly at the beginning of sintering, and become flat as the holding time increases after 1000min. This is caused by the release of the system's surface energy. When sintering starts, the surface energy is large and it is eager to decrease, resulting in the high decreasing rate of the porosity. As holding time increases, the particles coalesce to form grains and the surface energy is lower than the beginning, thus the decreasing rate of porosity is slower and the curves become smooth.

In the early stage of sintering, the temperature is low and surface diffusion plays an important role. In this stage, atoms move to the necks between two contacting particles through the surface. As temperature increases, bulk diffusion starts to play an important role. Due to the void concentration gradient, atoms start diffusion from the interior to the necks. The necks then grow into the space which makes the pores surrounded by three grains. The pores transform into a tunnel-shape connecting to other pores. In this stage, atoms occupy the voids through bulk diffusion and grain boundary diffusion, which leads the pores to shrink and some small pores may even disappear. Grain boundaries start to move and grains start to grow. The velocity of grain boundaries depends on the curvature of grain boundary and the temperature.

During sintering, the pores will move onto the grain boundaries. At first there are a large number of pores on the grain boundaries, preventing them from moving. As sintering goes further, the number of pores decreases and could not stop grain boundaries from moving. Thus the grain boundaries will bring the pores to move together and the pores are still on the

grain boundaries. In this stage, some pores may move out of the body through the grain boundaries which leads to the decrease of porosity, but some pores may move together to form a larger pore, which leads to the pore size increasing and the number of pores decreasing. If the temperature continuously increases, the grain boundaries will move faster skipping the pores and leaving them inside the grains, which will cause difficulty in densification.

Besides, the porosity is also related to the pressure inside the pores. During sintering, a pore will shrink if it does not meet any other pores while moving, and the pressure in this pore will increase. When the pressure in the pores increases and equals to the sintering driving force, the sintering process will stop. If the temperature is still increasing, the pressure in the pores will increase and the pores will start expanding leading to large porosity.

The coupons sintered at 1250℃ are cut into two pieces along the direction they were built up during the previous 3D printing step. OM graphs of the central parts are taken at different magnifications. The groups of graphs which are taken at 200x magnification are listed in Figure 5.6 below.

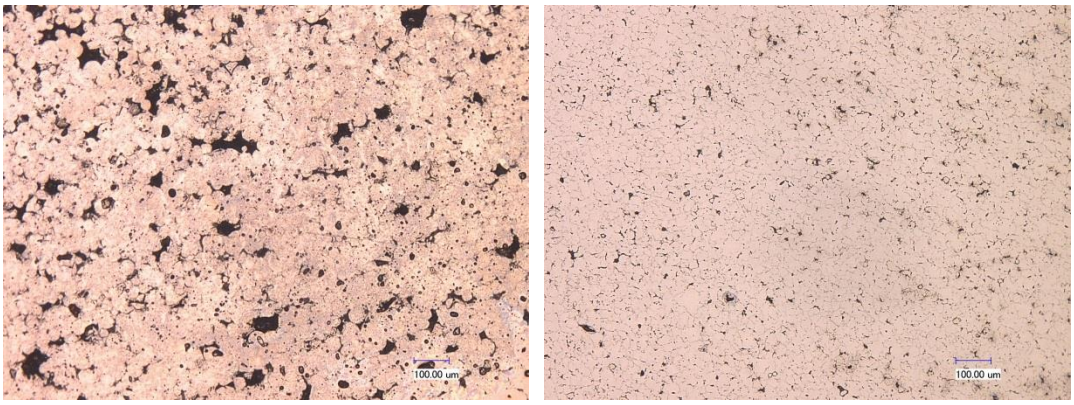

a(1) b(1)

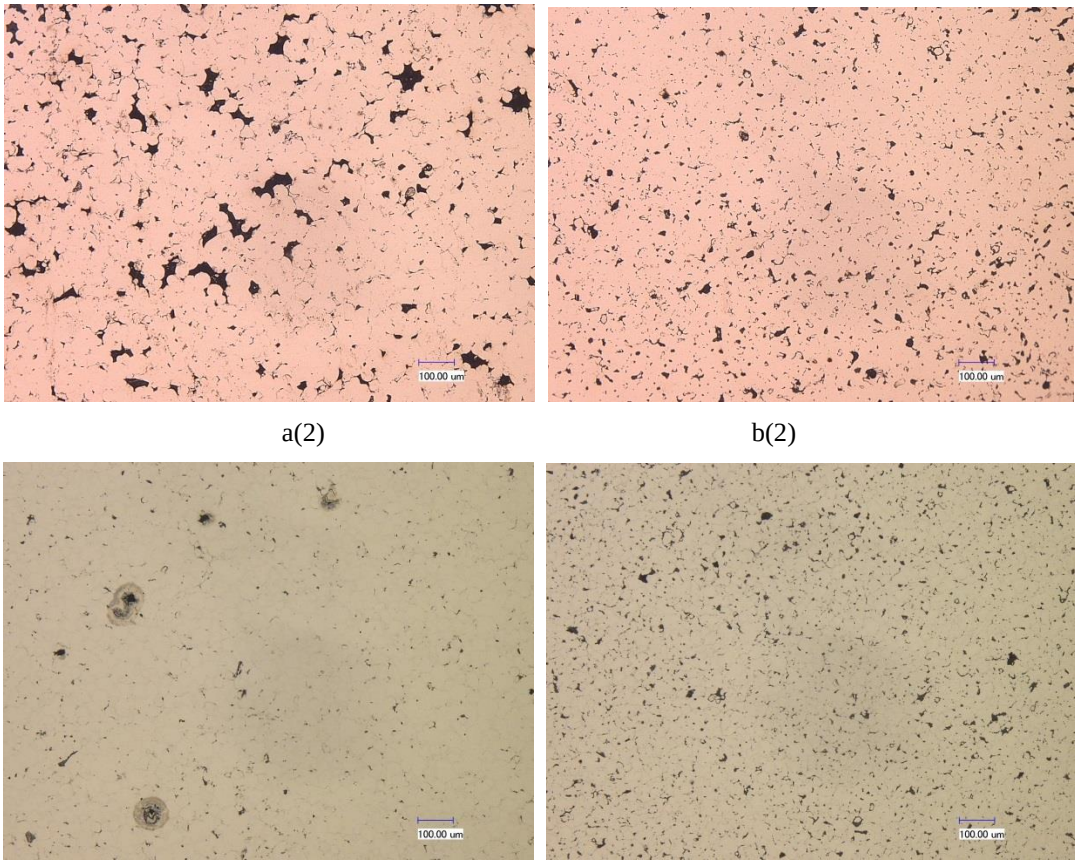

a(2) b(2)

a(3) b(3)

Figure 5.6 200x magnification OM images of central parts of coupons made of gas- and water atomized powder sintered at 1250 ℃ at different holding times:
a(1) 540min for gas atomized coupon, b(1) 540min for water atomized coupon,
a(2) 1000min for gas atomized coupon b(2) 1000min for water atomized coupon,
a(3) 1200min for gas atomized coupon, b(3) 1200min for water atomized coupon.

Figure 5.6 shows a series of OM graphs of gas atomized coupon and water atomized coupon at 1250 ℃ with different holding times. Figures from a(1) to a(3) show how sintering goes as the holding time increases of gas atomized coupon, and b(1) to b(3) show it of water atomized coupon. The area porosity calculation has also been done by Image J, and the data are shown in the following table:

Table 5.4 Area porosity changes at 1250 ℃ at various holding time

Powder type / Time	Gas atomized coupon porosity	Water atomized coupon porosity
540min	14.61%	6.95%
1000min	7.68%	6.62%
1200min	2.69%	6.14%

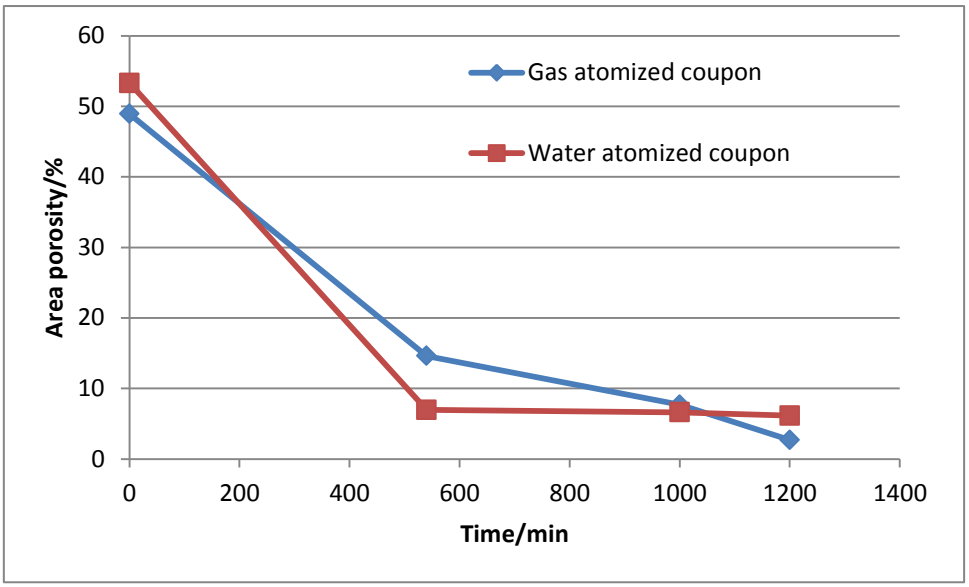

Figure 5.7 Area porosity vs Holding time relationship of gas atomized coupons and water atomized coupons at 1250 ℃

Figure 5.7 comes from the data in Table 5.4. From a(1) to a(3) in Figure 5.6, an obvious decreasing in area porosity of the central part can be observed, showing that most of the pores are moving out of the body through the grain boundaries from the center to the surface. From b(1) to b(3), the area porosity is always in a low percentage and does not show obvious changes. This is because water atomized coupon contains larger surface energy

which leads to faster sintering rate. The driving force of sintering process has been almost equal to the pressure inside the pores.

The curves in Figure 5.7 show that the area porosity of gas atomized coupon drops dramatically as the holding time increases, while the area porosity of water atomized coupon drops very slowly. This is the same as Figure 5.5 explains. Gas atomized powder has a regular shape, therefore the surface energy is low and the sintering goes slowly. Thus, the pores in gas atomized powder are still moving. But water atomized powder has an irregular shape with large surface energy and sintering goes much faster, so the sintering has almost stopped after certain time. Generally, the porosity decreases as the holding time increases, and both gas atomized powder and water atomized powder behave in this way. The difference between the area porosity in the center part and the body porosity shows the inhomogeneous distribution of the pores, illustrating that the pores move from the center to the surface, which is also observed in Graham's research about sintering titanium using 3D Printer for shaping [40]. However, when the holding time increases to 1200min, the area porosity of gas atomized coupon in the center reaches 2.69% while this porosity of the water atomized coupon is 6.14%.

In summary, at 1250℃ water atomized coupons are much easier to sinter than gas atomized coupons due to the larger surface energy, and the pores move from the center to the surface during sintering.

5.2.2 Porosity at 1300 ℃

The data of shrinkage, density and porosity are listed in Table 5.5, and the porosity change against the holding time is plotted in Figure 5.8.

Table 5.5 Shrinkage percentage, density and porosity of gas atomized and water atomized coupons after sintering at 1300 ℃

	540min gas	540min water	1200min gas	1200min water
Shrinkage(%)	23.03	44.03	29.90	48.07
Density(g/cm^3)	4.99	6.28	5.48	6.76
Porosity(%)	35.62	18.97	29.30	12.78

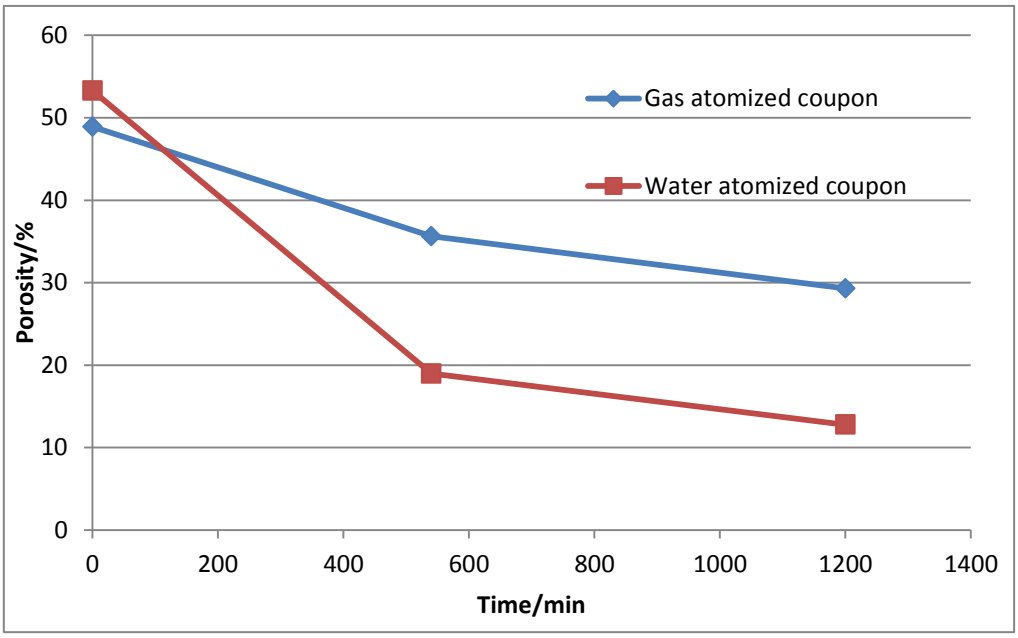

Figure 5.8 Porosity change against holding time for gas- and water-atomized coupons at 1300 ℃

From Table 5.5 and Figure 5.8, both gas- and water-atomized coupons obtain lower porosity. Water atomized coupon still sinter faster than gas atomized powder. From Figure 5.5 and Figure 5.8, when temperature increases only for 50 ℃, the porosity of gas atomized coupon has decreased about 10% and porosity of water atomized coupon has decreased about 8%, but as the sintering holding time increases, the decreasing rate of porosity is slower and slower. This tells us that by increasing the holding time, eventually the porosity will stop decreasing. If lower porosity is expected, temperature should be raised up.

Coupons after 1300 ℃ sintering are also cut into two pieces and the central part OM graphs have been taken and listed in Figure 5.9.

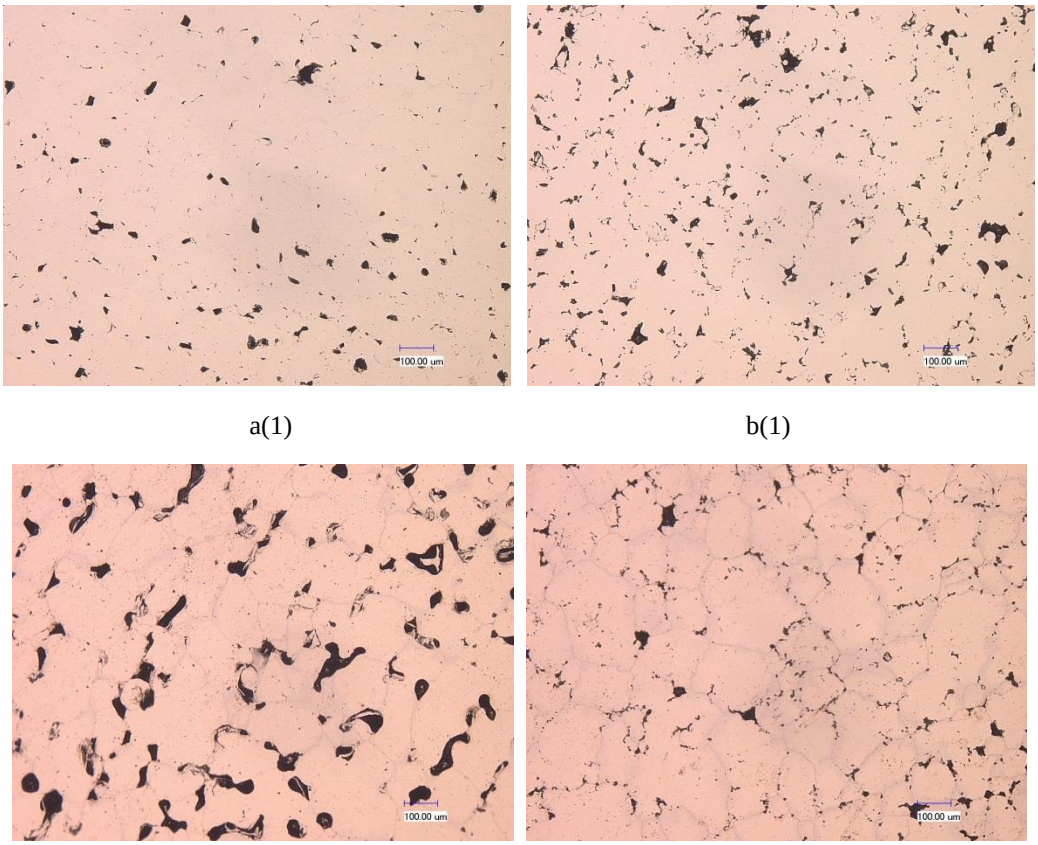

a(1) b(1)

a(2) b(2)

Figure 5.9 200x magnification OM pictures of gas atomized powder and water atomized powder at 1300 ℃ at different holding time:
a(1) 540min for gas atomized powder, b(1) 540min for water atomized powder,
a(2) 1200min for gas atomized powder, b(2) 1200min for water atomized powder.

Figure 5.9 shows another series of OM pictures of gas atomized coupon and water atomized coupon at 1300 ℃ at different holding time of 540min and 1200min. Comparing a(1) with a(2), an obvious increasing area porosity of gas atomized powder can be observed, especially a(2), showing that the pores seems get together while moving and become large pores. Comparing b(1) with b(2), the area porosity of water atomized coupon decreases a little, similar to 1250 ℃. The area porosity analysis is calculated and the data are put in the following table:

Table 5.6 Area porosity changes at 1300 ℃ at various holding times

Powder type / Holding time	Gas atomized powder porosity	Water atomized powder porosity
540min	2.67%	5.32%
1200min	9.12%	3.93%

From Table 5.6, the area porosity of water atomized powder at 1300 ℃ holding for 540min is 5.32% and it decreases a little to 3.93% when the holding time increases to 1200min, which is similar to the coupons at 1250 ℃ that the water atomized powder has almost stopped sintering, so the pores do not move very often. The area porosity of gas atomized powder at 1300 ℃ holding for 540min is 2.67%. However, the porosity greatly increases to 9.12% when the holding time is 1200min. This means the pores in gas atomized coupon grow and many pores coalesce together and do not move out to the surface.

The porosity in the center position is much lower than the porosity of the whole part at 1300℃, as same as it shown at 1250℃. This difference of porosity shows that the pores tend to move from the center to the surface and most of the pores are near the surface after sintering.

5.3 MICROSTRUCTURE CHANGE IN SINTERING

In general, the porosity will decrease during sintering process. As explained before, the pores are connected together like tunnels in early sintering. They will move along the grain boundaries and most of them can be eliminated out of the green body by grain boundaries movements. Meanwhile, large pores will grow by two or more small pores "meeting together" during sintering while small pores consumes.

In order to study the microstructure change of pores behaviors in the previous sintering processes, the average pore size and the number of pores per unit area has been analyzed as the following tables show:

Table 5.7 Pore behavior analysis data of gas atomized coupon at 1250℃

	540min	1000min	1200min
Average pore size/μm^2	24.291	21.804	12.769
No. of pores per unit area/mm^{-2}	6015.81	3507.59	2102.94

Table 5.8 Pore behavior analysis data of water atomized coupon at 1250 ℃

	540min	1000min	1200min
Average pore size/μm^2	12.215	20.060	22.171
No. of pores per unit area/mm^{-2}	3244.94	2275.29	2120.43

Table 5.9 Pore behavior analysis data of gas and water atomized coupon at 1300 ℃

	540min gas	540min water	1200min gas	1200min water
Average pore size/μm^2	42.152	23.187	80.023	20.181
No. of pores per unit area/mm^{-2}	1067.07	2292.14	1139.04	1944.79

Using the data from Table 5.7-5.9, a series of relationships between pore behavior and sintering parameters can be built.

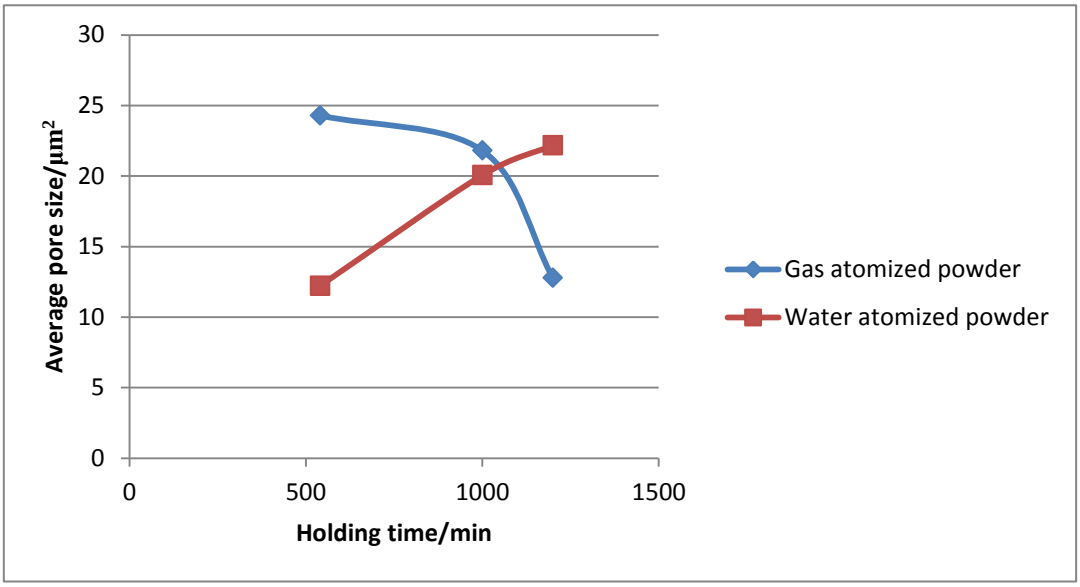

Figure 5.10 Relationship between average pore size and holding time for both gas and water atomized powder at 1250 ℃

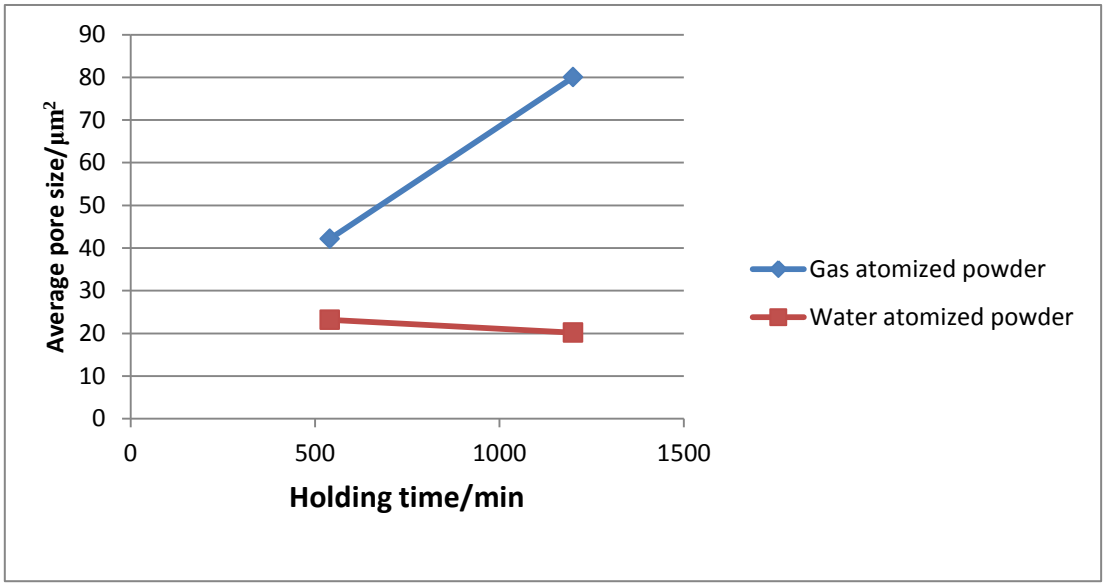

Figure 5.11 Relationship between average pore size and holding time for both gas and water atomized powder at 1300 ℃

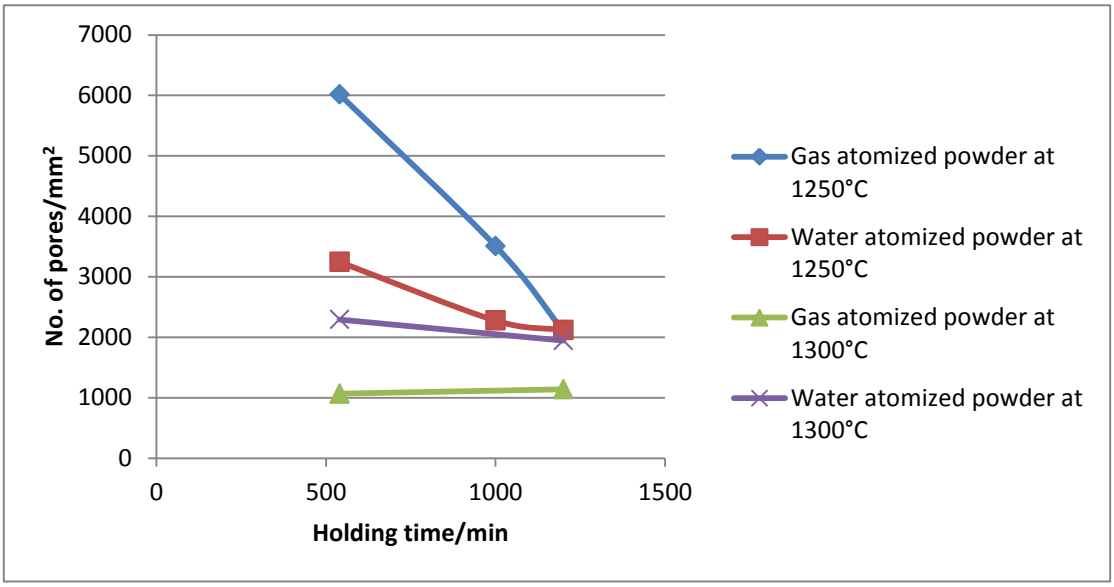

Figure 5.12 Relationship between number of pores per unit area and holding time at different temperatures.

Relationships between the average pore size, the number of pores per unit area and the sintering temperature and holding time has been illustrated from Figure 5.10 to 5.12. From Figure 5.12, it can be observed that the number of pores per unit area decreases as the temperature increases, and also decreases as the holding time increases. This is normal because sintering is a densification process, during which most of pores are moving out of the body through grain boundaries. At 1250 ℃, the decreasing rate of pores number per unit area of water atomized coupon is much slower than it of gas atomized coupon. This is because the water atomized coupon has high surface energy and is easy to sinter. At 1250 ℃, the water atomized coupon has almost reached the final sintering point, so most of the pores do not move. The gas atomized coupon is still getting densification at a low rate, so the pores do not behave like water atomized coupon. The low decreasing rates of porosity and number of pores per unit area of water atomized coupon at 1250 ℃ state that the sintering process will almost finish. Most of the pores will not move and the green part will not get higher density even for longer holding time. At 1300 ℃ the number of pores per unit area remains

approximately stable as holding time increases for both water atomized coupon and gas atomized coupon. This tells us that the sintering is going to stop. Thus, holding for longer time would not get lower porosity at 1300 ℃ sintering.

From Figure 5.10 to 5.11, it can be also observed that the average pore size increases as temperature increases. This is not against to the porosity decreasing because the number of pores is also decreasing. At 1250 ℃, the average pore size of gas atomized powder decreases as holding time increases. This is because the pores are still moving, and the densification is slightly getting better. The average pore size of water atomized coupon increases, stating that the velocity of pore movement decreases and the sintering slows down. At 1300 ℃, the average pore size of water atomized coupon remains approximately stable which is similar to the pore numbers, telling us that the sintering process almost finishes or has already finished.

OM images at higher magnifications has also been taken and listed below:

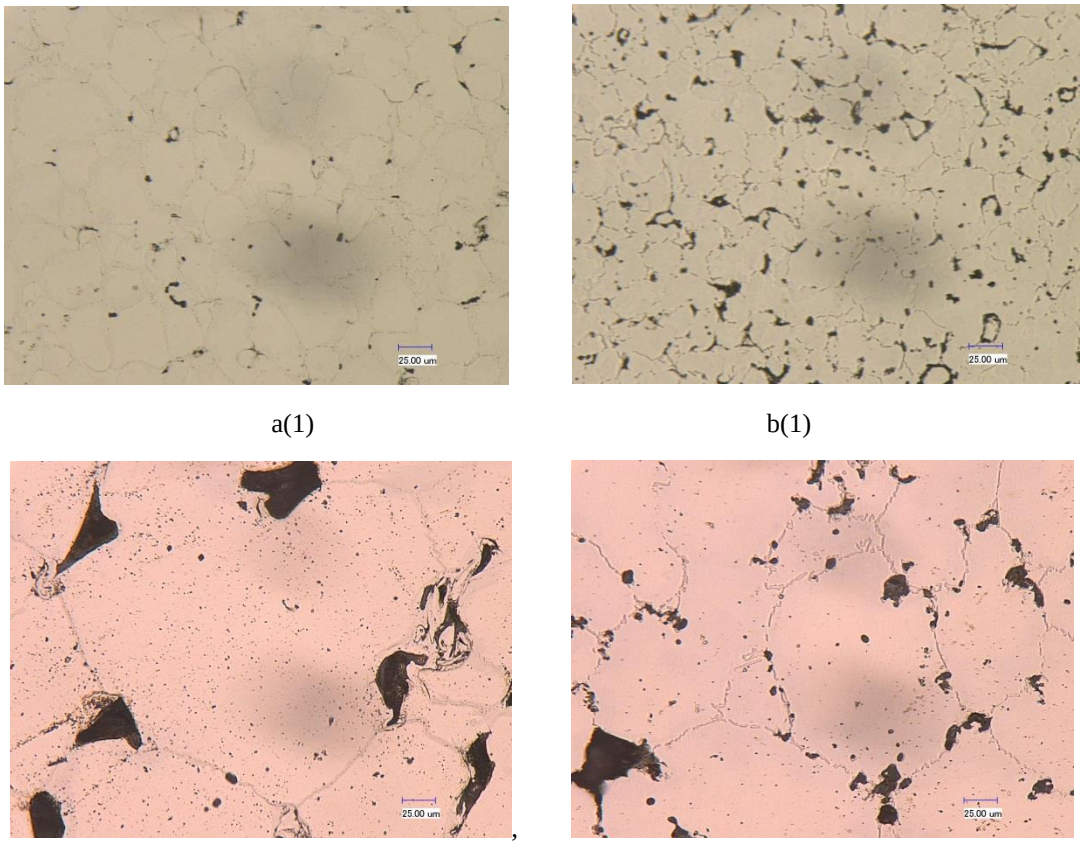

a(1) b(1)

a(2) b(2)

Figure 5.13 OM pictures for gas- and water-atomized coupon at different temperature holding for 1200min at a 800x magnification:
a(1) at 1250 ℃ for gas atomized coupon, b(1) same for water atomized coupon,
a(2) at 1300 ℃ for gas atomized coupon, b(2) same for water atomized coupon.

Figure 5.13 shows the OM pictures of gas atomized sample and water atomized sample for 1250 ℃ and 1300 ℃ at 800x magnification. It can be observed that the grains of 1300 ℃ coupons of both coupons grow much larger than the 1250 ℃ coupons, which is not good for mechanical properties according to Hall-Petch equation. What's more, the pores for both samples at 1250 ℃ are on the grain boundaries, but at 1300 ℃ some pores are in the grains. This may be due to the rapid grain boundary moving, skipping the pores and wrapping a lot of cores inside the grains because of local overheating. This is an undesirable

phenomenon because the properties will be pool. Thus, temperature control is very important during sintering.

5.4 OPTIMUM SINTERING PROCESS

For gas atomized powder, the best sintering result is provided by sintering at 1250℃ holding for 1200min due to the goal of densification. Under this condition, the porosity of the whole part is 38.59% and the porosity in the center is 2.69%. Even though the whole part porosity is higher than the porosity sintering at 1300℃ for 1200min (29.30%), the porosity of the center part is much lower than the porosity of that sintering process (9.12%). Since the porosity on or near the surface could be eliminated by cutting or even grinding, I would pick up the sintering process at 1250℃ holding for 1200min as the best result for gas atomized powder. The OM pictures in Figure 5.13 a(1) and a(2) show that sintering at 1250℃ for 1200min provides a better inner microstructure.

For water atomized powder, according to the porosity of the whole part and the center, the best sintering result of these five processes should be at 1300℃ holding for 1200min. In this processing, water atomized powder obtains a porosity of 12.78% and a center area porosity of 3.93%.

6.0 CONCLUSIONS AND FUTURE WORKS

6.1 CONCLUSIONS

This thesis examined the sintering behavior of stainless steel 420 coupons produced by the M-Flex 3D Printer. The introduction of additive manufacturing process to the green part building step provides accurate dimensional control, but requires higher temperature for sintering. Powders produced from gas atomization and water atomization are analyzed and applied to print the green bodies as a comparison. Sintering processes at different temperatures and different holding times have been done. The porosity change and the related microstructure change have been studied. The conclusions can be drawn in several points:

1. Water atomized powder can get much higher densification than gas atomized powder under same sintering conditions. This is due to its irregular shape and large surface area, which leads to large surface energy that drives the sintering process. Water atomized powder can be sintered to almost 90% densification at 1300℃ for 1200min, while gas atomization could only get about 70% densification. Thus, water atomized powder is easier to sinter, but the dimensions of it will change rapidly, which may cause difficulty in dimension control.

2. The center part shows higher densification than the whole coupon. This means that the pore distribution is inhomogeneous during sintering stainless steel 420

produced by the M-Flex 3D Printer. Most of the pores tend to move out of the body during sintering.

3. 1300℃ is not higher enough according to the results. Since no external pressure is applied during the shaping step by 3D Printer, the sintering temperature for this method may need to go higher.

4. Atom diffusion in solid state plays an important role in the sintering process. Increasing holding time in the early sintering may help to get higher density, but eventually the porosity will stop decreasing. In addition, longer holding times at elevated temperatures causes grain coarsening, hence the standard mechanical properties in terms of yield strength and ultimate tensile strength will be expected to decrease. Thus, certain holding time is necessary, but long-term holding is not suggested. Compared to holding time, temperature is the dominant factor for sintering.

5. Even the samples are encapsulated in a vacuum quartz tube to avoid oxidation, it is still not real vacuum because the tube is sealed. Once the air in the pore comes out, it is not able to extract the air away. Though such small amount of air will not cause oxidation in these experiments, there will always be some air in the open pores, which will prevent the part from getting full density. Thus, real vacuum condition with a vacuum pump is worth trying.

6.2 FUTURE WORKS

The present study is the first step in understanding the sintering behavior of parts made using 3-D printing. Additional works need to be done to continue developing the basic knowledge of sintering and to improve the properties.

In order to get higher densification, higher temperature experiments need to be run. Since the sintering stops when the driving force is equal to the pressure inside the pores, real vacuum condition can be applied to extract the air out of the furnace during sintering until it gets full densification. Also controlled atmospheres that prevent the oxidation of the parts will be explored. However, cautions need to be taken to the evaporation of chromium in stainless steel which will greatly decrease the corrosion-resistant property. Another worth trying way is to mix smaller size powder together to fill in the spaces between the large powders, or directly use smaller size powder to increase the green part density. Hot isostatic pressing and infiltration can also be tried to achieve theoretical density.

Another inverse thought to produce materials with both porous structure and enough strength is also worth trying. If the porosity could be engineered for stainless steel or other materials, there will be more applications such as thermal transfer materials, shock absorption materials and sound insulation materials. Experiments with different atmospheres, temperatures, holding times, particle shapes and sizes need to be done to build a map to show the relationships between porosity and other parameters to achieve engineered porosity.

BIBLIOGRAPHY

[1] Campbell, John. *Castings*. 2nd ed. Berwick: Reed Educational and Professional Publishing, 1993.

[2] Campbell, James S. *Casting and Forming Processes in Manufacturing*. 1st ed. New York: McGraw-Hill, 1950.

[3] Lea, Frederick Charles, and Eric, N. Simons. *The machining of steel, a simple explanation of its principles and practice*. 2nd ed. London: Odhams Press, 1960.

[4] Moyer, James Ambrose. *Welding*. 1st ed. New York & London: McGraw-Hill book company, inc., 1942.

[5] German, Randall M. *Powder Metallurgy of Iron and Steel*. Canada: John Wiley & Sons, Inc., 1998.

[6] German, R. M. and Bose, A. *Injection Molding of Metals and Ceramics*. Princeton, NJ: Metal Powder Industries Federation, 1997.

[7] Pavan Suri, Ryan P. Koseski, and Randall M. German. *Microstructural evolution of injection molded gas- and water-atomized 316L stainless steel powder during sintering*. Materials Science & Engineering A(402). pp.341-348, Jan. 2005.

[8] E. Klar and J. W. Fesko. Gas and Water Atomization, *Powder Metallurgy*. Metal handbook. 9th ed. American society for Metals, vol. 7, pp.26, 1984.

[9] Erhard Klar and Prasan K. Samal. *Powder Metallurgy Stainless steels Processing, Microstructures, and Properties*. Ohio: ASM International, 2007.

[10] ASM Handbook Committee. *Powder Metal Technologies and Applications*. Ohio: ASM International, 1998

[11] B. B. Mandelbrot. *The Fractal Geometry of Nature*. 1st ed. New York: W.H.Freeman & Company, 1982.

[12] M. Fernandez-Martinez and M. A. Sanchez-Granero. *Fractal dimension for fractal structures*. Topology and its Applications. vol. 163. pp. 93-111, 2014.

[13] Schneider, Joel E. *A Generalization of the Von Koch Curve*. Mathematics Magazine, vol. 38. pp. 144-147, May. 1965.

[14] Larry S. Liebovitch and Tibor Toth. *A Fast Algorithm to Determine Fractal Dimensions by Box Counting*. Physics Letters A. vol. 141. no. 8,9. pp. 386-390, Nov. 1989.

[15] T. Hartwig, G. Veltl, F. Petzoldt, H. Kunze, R. Scholl and B. Kieback, *Powders for Metal Injection Molding*. Journal of the European Ceramic Society. vol. 18. pp. 1211-1216, 1998.

[16] A. Shirizly, J. Tirosh and L. Rubinski. *Densification Process of Porous Materials Under Uniaxial Compression*. International Journal of Damage Mechanics. vol. 16. no. 4. pp. 427-455, Oct. 2007.

[17] Fang, Zhigang Zak. *Sintering of Advanced Materials*. Great Abington: Woodhead Publishing, 2010.

[18] Kang, Suk-Joong L. *Sintering: Densification, Grain Growth and Microstructure*. Burlington: Butterworth-Heinemann, 2005.

[19] M. I. Alymov, S. I. Averin and V. S. Shustov. *Sintering Mechanisms for Crystalline Powders: Comparative Analysis*. International Journal of Self-Propagating High-Temperature Synthesis. vol. 22. no. 4. pp. 234-235, 2013.

[20] Andrej Salak. *Ferrous Powder Metallurgy*. Great Abington: Cambridge International Science Publishing, 1995.

[21] G. H. Gessinger. *Powder Metallurgy of Superalloys*. Cambridge: Butterworth & Co., 1984.

[22] A. J. Sharler and John Wulff. *Mechanism of Sintering*. Industrial and Engineering Chemistry, vol.40, no.5, pp.838-842, May. 1948.

[23] Hirota Noriaki, Yin Fuxing, Azuma Tsukasa and Inoue Tadanobu. *Yield stress of duplex stainless steel specimens estimated using a compound Hall-Petch equation*. Science and Technology of Advanced Materials. vol. 11. p. 025004, Apr. 2010.

[24] C. C. Degnan, P. Jackson, D. P. Weston and J. V. Wood. *Reactive sintering of stainless steel*. Materials Science and Technology. vol. 17. pp. 1624-1634, Dec. 2001.

[25] O. Ertugrul, H. S. Park, K. Onel and M. Willert-Porada. *Effect of particle size and heating rate in microwave sintering of 316L stainless steel. Powder Technology*. vol. 253. pp. 703-709, Feb. 2014.

[26] Shishir Pandya, K. S. Ramakrishna, A. Raja Annamalai and Anish Upadhyaya. *Effect of sintering temperature on the mechanical and electrochemical properties of austenitic stainless steel.* Materials Science & Engineering A(556). pp. 271-277, 2012.

[27] R. Mariappan, S. Kumaran and T. Srinivasa Rao. *Effect of sintering atmosphere on structure and properties of austeno-ferritic stainless steel.* Materials Science & Engineering A(517). pp. 328-333, 2009.

[28] S. M. Tiwari, S. Balaji, A. Upadhaya. *Sintering and characterization of YAG dispersed ferritic stainless steel.* Materials Science & Engineering A(492). pp. 60-67, 2008.

[29] Matsuura Kiyotaka, Sueoka Noritoshi, Kudoh Masayuki and Ohsasa Kenichi. *Nickel monoaluminide coating on ultralow-carbon steel by reactive sintering.* Metallurgical and Materials Transactions A, Physical Metallurgy and Materials Science, vol. 30. pp. 1605-1612, 1999.

[30] Nakamoto Takayuki, Shirakawa Nobuhiko, Miyata Yoshio and Inui Haruyuki. *Selective laser sintering of high carbon steel powders studied as a function of carbon content*. Journal of Materials Processing Technology, vol. 209. pp. 5653-5660, 2009.

[31] Rottger A., Weber S. and Theisen W. *Supersolidus liquid-phase sintering of ultrahigh-boron high-carbon steels for wear-protection applications*. Materials Science and Engineering A, vol. 532, pp. 511-521, Jan. 2012.

[32] Abosbaia A. A. S., Mitchell S. C., Youseffi M. and Wronski A. S. *Liquid phase sintering, heat treatment and properties of ultrahigh carbon steels*. Powder Metallurgy, vol.54, pp. 592-598, 2011.

[33] Oro R.,Campos M. and Torralba, J. M. *Study of high temperature wetting and infiltration for optimizing liquid phase sintering in low alloy steels*. Powder Metallurgy, vol. 55, pp. 180-190, Jul. 2012.

[34] Tougas B., Blais C, Chagnon F. and Pelletier S. *Effects of additions of nickel nanoparticles on sintering response of PM hybrid low alloy steels*. Powder Metallurgy, vol.56, pp.46-54, Feb. 2013.

[35] Weber S. and Theisen W. *Optimised sintering route for cold work tool steels*. Powder Metallurgy, vol. 49, pp. 355-362, Dec, 2006.

[36] Pellizzari M., Zadra M. and Fedrizzi A. *Development of a hybrid tool steel produced by spark plasma sintering*. Materials and Manufacturing Processes, vol. 24, pp. 873-878, Jul. 2009.

[37] Altun-Ciftcioglu Gokcen A., Ersoy-Mericboyu Aysegul and Henderson Clifford L. *Stochastic modeling and simulation of photopolymerization process*. Polymer Engineering & Science, vol. 51, pp. 1710-1719, Sep. 2011.

[38] I. Gibson, D. W. Rosen and B. Stucker. *Additive Manufacturing Technologies Rapid Prototyping to Direct Digital Manufacturing*. New York: Springer Science + Business Media, LLC, 2010.

[39] J-P Kruth, P. Mercelis, J. Van Vaerenbergh, L Froyen and M. Rombouts. *Binding mechanisms in selective laser sintering and selective laser melting.* Rapid Prototyping Journal, vol.11, pp.26-36, 2005.

[40] Graham Gagg, Elaheh Ghassemieh and Florencia Edith Wiria. *Effects of sintering temperature on morphology and mechanical characteristics of 3D printed porous titanium used as dental implant*. Materials Science and Engineering C, vol.33, pp. 3858-3864, 2013.

[41] Rasband, W. S., ImageJ, U.S. National Institutes of Health, Bethesda, Maryland, USA, http://imagej.nih.gov/ij/, 1997-2014.

[42] Karperien, A., FracLac for ImageJ. http://rsb.info.nih.gov/ij/plugins/fraclac/FLHelp/Introduction.htm. 1999-2013.